REPORT DOCUMENTATION PAGE

Form Approved OMB No. 0704-0188

1. REPORT DATE *(DD-MM-YYYY)*	2. REPORT TYPE	3. DATES COVERED *(From – To)*
25-01-2005	Final Report	1 December 2003 - 25-Jan-05

4. TITLE AND SUBTITLE

III-V/II-VI Hybrid Quantum Well Mid-Infrared Lasers

5a. CONTRACT NUMBER
FA8655-03-D-0001, Delivery Order 0013

5b. GRANT NUMBER

5c. PROGRAM ELEMENT NUMBER

6. AUTHOR(S)

Professor Maya Mikhailova

5d. PROJECT NUMBER

5d. TASK NUMBER

5e. WORK UNIT NUMBER

7. PERFORMING ORGANIZATION NAME(S) AND ADDRESS(ES)

A.F.Ioffe Physical-Technical Institute
26 Politekhnicheskaya St,
St. Petersburg 194021
Russia

8. PERFORMING ORGANIZATION REPORT NUMBER

N/A

9. SPONSORING/MONITORING AGENCY NAME(S) AND ADDRESS(ES)

EOARD
PSC 802 BOX 14
FPO 09499-0014

10. SPONSOR/MONITOR'S ACRONYM(S)

11. SPONSOR/MONITOR'S REPORT NUMBER(S)
EOARD Task 03-9006

12. DISTRIBUTION/AVAILABILITY STATEMENT

Approved for public release; distribution is unlimited.

13. SUPPLEMENTARY NOTES

14. ABSTRACT

This report results from a contract tasking A.F.Ioffe Physical-Technical Institute as follows: High-power mid-infrared semiconductor lasers are of great importance for many applications such as laser diode spectroscopy , pollution monitoring, low-loss optical communication, medical diagnostics, etc. This project will introduce quantum wells into a heterojunction structure, as a means of obtaining near-room-temperature, high power, mid-IR laser sources. Both experimental performance and means of fabrication will be investigated.

15. SUBJECT TERMS
EOARD, semiconductor devices, Quantum Well Devices, infrared technology

16. SECURITY CLASSIFICATION OF:			17. LIMITATION OF ABSTRACT	18, NUMBER OF PAGES	19a. NAME OF RESPONSIBLE PERSON
a. REPORT	b. ABSTRACT	c. THIS PAGE			DONALD J SMITH
UNCLAS	UNCLAS	UNCLAS	UL	36	19b. TELEPHONE NUMBER *(Include area code)* +44 (0)20 7514 4953

Final Technical report
on the project
“III-V/II-VI hybrid quantum well mid-infrared lasers”

Project manager **Maya P. Mikhailova, Dr.Sci.**

CRDF project RPO-1407-ST-03

Work period **12 months (December 2003 - November 2004)**

A.F.Ioffe Physico-Technical Institute
Saint Petersburg
Russia

2004

NOMENCLATURE PAGE

Key persons:

Yury P. Yakovlev, Deputy P.I., Dr.Sci., p.r.s.
Albert N. Imenkov, Dr.Sci., l.r.s.
Alexsander N. Titkov, Dr.Sci., p.r.s.
Georgii G. Zegrya, Dr.Sci., s.r.s.
Konstantin D. Moiseev, Ph.D., s.r.s.
Vadim P. Evtikhiev, Ph.D., s.r.s.

Investigators:

Alexander V. Ankudinov, Ph.D., r.s.
Eduard V. Ivanov, Ph.D., r.s.
Sergey S. Kizhaev, Ph.D., r.s.
Alexei S. Shkolnik, Ph.D., r.s.
Marina G. Rastegayeva, Ph.D., r.s.
Sergey S. Molchanov, r.s.
Elena A. Grebenshchikova, r.s.
Anastasia P. Astakhova, j.r.s.
Tatyana I. Kachalova, eng.

P.I. – principal investigator
l.r.s. – leader research scientist
p.r.s. – principal research scientist
s.r.s. – senior research scientist
r.s. – research scientist
j.r.s. – junior research scientist
eng. – engineer

SUMMARY

The main goal of the project is to fabricate the asymmetric mid-ir laser structure with various width of quantum well in an active region and to investigate laser parameters. New physical and technological approaches are proposed consisting in combining III-V/II-VI compounds InAsSbP/InAsSb/CdMgSe growing by LPE (III-V part) + MBE (II-VI part) technology. Morphology of the laser structures and surface potential profiles were studied by modified AFM method. Spontaneous and coherent emissions were studied. Lasing at λ=3.5 μm was achieved in pulse regime at 80 K and threshold current density J_{th}=4 kA/cm^2 was obtained. Optical confinement and lasing spreading in an active region was calculated. The proposed approach allows one to achieve large band offsets (ΔEc, ΔEv) and to provide a good good carrier and optical confinement. Low threshold current and weak temperature dependence are expected. Quantum well laser structures with single and triple AlSb/InAsSb/AlSb quantum wells were grown by MOVPE and their electroluminescence properties were studied in the range T=77-300 K. Theoretically calculation of energy spectrum of QWs and radiative and non-radiative recombination transitions in an asymmetric quantum well were performed. MOCVD technology was developed to grow DH InAsSb/InAsSbP lasers structures with high phosphorous content (P~50%) in cladding layer. Electroluminescence was studied at 77-300 K in dependence on P content in solid phase. Coherent emission at λ=3.1 μm was observed at 77 K. Wide gap confined layers AlGaAsSb were grown on InAs by MBE, and conditions for quality grown of these layers were determined. Original combine technology of growing InAsSbP/InAsSb/AlAsSb heterostructures with quantum well in an active layer by two-steps MOCVD was developed to get a large band offset ΔEc=1.2 eV. Intense spontaneous emission in the range 3-4 μm was observed at 77-300 K. The heterostructures Proposed in the frame of the project are very attractive for design high-power infrared lasers operating near room temperature.

INTRODUCTION

The proposed project is devoted to the development of nanotechnology and study of luminescent properties of narrow-gap heterostructures with asymmetric quantum wells and superlattices as an active region of mid-ir laser structures operating in the range of 3-5 μm at room temperature.

Mid-infrared semiconductor lasers are of great importance for many applications such as laser diode spectroscopy, pollutant monitoring, low-losses longwavelength optical communication, medical diagnostics etc [1-4]. Narrow-gap III-V semiconductor heterostructures are very attractive for this purpose due to simple enough fabrication technology and to much more high optical power than that of the lead-salt based lasers whose typical maximum output power is only 1 mW [5]. On the other hand, the narrow-gap III-V lasers have some disadvantages due to non-radiative recombination losses, intravalence band absorption and carrier leakage from the active region [6,7].

Recently we have proposed some new physical approaches to design an energy band structure of mid-infrared lasers in order to improve their parameters. One of them consists of using type a type II broken-gap heterojunction in the active region of the laser to decrease Auger-recombination and to reduce injection current [8,9].

Another approach was proposed in the project under EOARD contract N F61775-99-WE016 [10]. Theoretical model of laser structure with high (more than 3-5 kT) asymmetric barriers for electrons and holes at the interfaces between narrow-gap quantum well (QW) active layer and wide-gap cladding layers was offered which can combine the advantages of both type I and type II lasers. In the type I structure quantum well active layer is sandwiched between wide-gap N- and P-cladding materials forming a type II heteropair. This approach allows the carrier leakage from the active region of the laser structure, especially hole leakage, to be reduced. In the type II heterojunction consisting of wide-gap semiconductors N and P-type narrow band gap quantum-size active layer is built-in (for example in n-InAs(Sb)) which forms type I heterojunction with confined layers. This quantum-size layer forms asymmetric barriers of different height at heteroboundaries owing to band offsets in valence and conduction bands. Such barriers prevent majority carrier injection and reduce current losses in laser structure.

In the framework of the previous project (EOARD contract 007036, ISTC project N 2044p) we proposed a design of asymmetric heterostructure for fabrication high power, high temperature operating mid-infrared lasers [11]. This approach consisted of the combining of III-V and II-VI compounds in one laser structure based on Al(Ga)SbAs/InAs/CdMgSe heterostructure grown by MBE. It allowed to achive large band offsets ΔE_c, ΔE_v to obtain pseudomorphic laser structure and to reach strong optical confinement [12,13].

Then, using III-V compound only that allows keeping the laser structure in the “6.1 Å” family (InAs, GaSb, AlSb) and their heterostructures (according to H.Kroemer determination [14]), we can improve heterointerface morphology and obtain better performance of laser structures. As an alternative way a fabrication and study of asymmetric double heterostructure InAsSbP/InAs/InAsSbP grown by MOCVD with high P content (P>~50%) was included [15,16].

The following main results were obtained in the frame of preceding EOARD project:

- novel hybrid laser structure based on III-V/II-VI compounds with strong asymmetric band offsets was proposed, fabricated and studied. Pseudomorphic AlGaAsSb/InAs/CdMgSe structure was grown in two subsequent MBE processes.

- first observation of stimulated emission at λ=2.775 μm was achieved for the hybrid p-AlAsSb/n^0-InAs/n-CdMgSe laser structures at 80 K with threshold current density J_{th}=4 kA/cm^2.
-MOVPE technology of InAsSbP/InAs/InAsSbP laser structures with high P content (>~50%) was developed. High efficiency light-emitting diodes have been fabricated for the specral range λ=3-4.5 μm, single-mode lasing with λ=3.04 μm have been obtained in pulse mode at T=80 K.

The following main tasks were determined for the future study and were solved in the frame of the current project:
- complex study and optimization of hybrid III-V/II-VI heterostructure based on InAsSb/CdMgSe to shift specral range of laser emission up to 3-4 μm and to improve morphology and interface III-V/II-VI interface quality. It allows to increase operating temperature and to suppress current leakage. For these purposes new hybrid structures grown by combine LPE+MBE method will be proposed. Using LPE method for growing III-V part allows to get lattice-matched heterostructure and to reduce defects density at the InAsSb/CdMgSe interface.
- characterization of the hybrid structures by improved AFM methods (Kelvin probe, microscope study)
- the creation of quantum well AlSb/InAsSb/AlSb laser heterostructures with various width of the active region. Theoretical study of recombination processes in these QW structures;
- MOCVD growing of InAsSb/InAsSbP laser heterostructures with high P content will be developed. To get a large conduction band offset a new original method of growing wide-gap InAsSbP/InAsSb laser heterostructure by two-step MOCVD process was proposed and realized.

According the Work Plan the following results were obtained in the frame of the current project:
1. Asymmetric hybrid III-V/II-VI AlGaAsSb/InAsSb/CdMgSe laser structure was grown by combination of two technological methods LPE(III-V) and MBE(II-VI).
2. Morphology of laser facets and surface potential profile distribution of laser structures were studied by a new AFM method (Kelvin probe microscopy).
3. Quantum well laser structures AlSb/InAsSb/AlSb were grown by MOCVD and its electroluminescence properties were studied. Characterization of these structures was made by AFM.
4. Theoretical study of longwavelength quantum well laser structure was performed including energy levels distribution in QW of InAsSb and analysis of radiative recombination processes.
5. Wide-gap AlGaAsSb and InAsSbP layers as confinements of laser structures were grown on InAs substrates by MBE and MOCVD respectively.
6. MOCVD technology was developed to grow DH InAsSb/InAsSbP laser structure with high P content in the cladding layer. Photoluminescence and electroluminescence were studied at 77-300 K in dependence on P content.
7. Original combine technology for growing InAsSbP/inAsSb/AlGaSb laser structures in two-step MOCVD process was used to increase the conduction band offset at the InAsSb/AlGaSb interface and to improve laser performance.

Work plan of the project

I quarter. (December 2003 – February 2004)
Hybrid InAsSbP/InAsSb/CdMgSe laser structures grown by combine technology method LPE + MBE.
1.1. Growing of InAsSbP/InAsSb/CdMgSe laser structure
1.2. Characterization of the laser structures and interface quality (STM, EPFM etc)
1.3. Study of spontaneous and coherent emission, temperature dependence of threshold current, polarization

II quarter. (March – May 2004)
Study and development quantum well structure as an active region for the spectral range 3-4 μm.
2.1. Growing of Ga(In)Sb/InAs(Sb) QWs with various line-up by MBE method on InAs substrate.
2.2. Characterization of the structure quality and luminescent properties study (PL, EL, etc).
2.3. Theoretical computation of superposition of radiative and non-radiative recombination rates in dependence on quantum well width and interface formation conditions.

III quarter. (June – August 2004)
Growing and study of wide-gap cladding layers for asymmetric laser structure.
3.1. Growing of InAsSbP layers with maximum content of phosphorus (P<60%) by MOCVD method. Characterization of heterointerface quality by STM, AFM etc.
3.2. Growing of AlGaAsSb epilayers be MBE method. Study of transport properties of the single heterostructure and the electron channel in InAs formed by doping level of AlGaAsSb epilayer.
3.3. Optical study of band offsets at the interfaces formed by various nanostructure technologies.

IV quarter. (September – November 2004)
Fabrication of hybrid QW laser structure growing by combine MOCVD + MBE method.
4.1. Growing of InAsSbP/InAsSb/AlGaAsSb laser structures
4.2. Study of spontaneous and coherent emission, temperature and polarization characteristics
4.3. Technical Report preparation.

TECHNICAL DESCRIPTION OF THE PROJECT

1. Hybrid InAsSbP/InAsSb/CdMgSe laser structures grown by combine technology LPE + MBE method.

1.1. Growing of InAsSbP/InAsSb/CdMgSe laser structure

The hybrid InAsSbP/InAsSb/CdMgSe laser structures were obtained by combine method using two separate epitaxial growth setups of liquid-phase epitaxy (III-V part) and molecule-beam epitaxy (II-VI part). The laser heterostructure was grown on a p^+-InAs(100) substrate with carrier concentration p~5×10^{18}cm^{-3}. The III-V part of the structure consisted of the 2 μm-thick wide-gap p^+-$InAs_{0.62}Sb_{0.12}P_{0.26}$ (E_G=0.527 eV) cladding layer heavy doped with Zn and 0.8 μm-thick narrow-gap n^0-$InAs_{0.92}Sb_{0.08}$ active region (E_G=0.347 eV) which was unintentionally doped. The LPE growth was carried out using a conventional horizontal slider graphite boat under purified hydrogen flow atmosphere. The wet pre-growth treatment of the InAsSb epilayer surface in a Na_2S-water solution was made before inserting into a MBE chamber [17]. The Na_2S wet chemical treatment improves the InAs-rich surface morphology replacing the oxide film on the InAsSb surface by an In-S overlayer and protect it from oxidation [18]. Then, the LPE grown heterostructure was loaded into the III-As MBE growth chamber connected to the II-VI MBE chamber through an UHV transfer tube for the annealing. The II-VI growth initiation in a low-temperature migration enhanced epitaxy mode was rather 2D than 3D [19]. The II-VI part of the structure consisted of 1.5 μm-thick n-$Cd_{0.9}Mg_{0.1}Se$ cladding layer (n~8×10^{17}cm^{-3}) lattice-matched to InAs and a heavy doped n^+-CdSe cap layer of 100 nm in a thickness both doped with Cl [12]. As a result, the InAsSbP and CdMgSe cladding layers forming type II heterojunction between them confine electrons and holes in the active region of the structure under study due to asymmetric band-offsets at the heteroboundary with the InAsSb active layer (Fig.1.1).

Double-channel mesa-stripe diodes were fabricated by a wet chemical etching using ordinary photolithographic technique. The stripe width and the cavity length of the samples under study were 50 μm and 250-500 μm, respectively. Ohmic contacts to p-InAs side and n^+-CdSe epilayer were formed by a high vacuum metal deposition using Cr and Au alloys. Laser diode chips were mounted on a copper heatsink and bound by an Au wire.

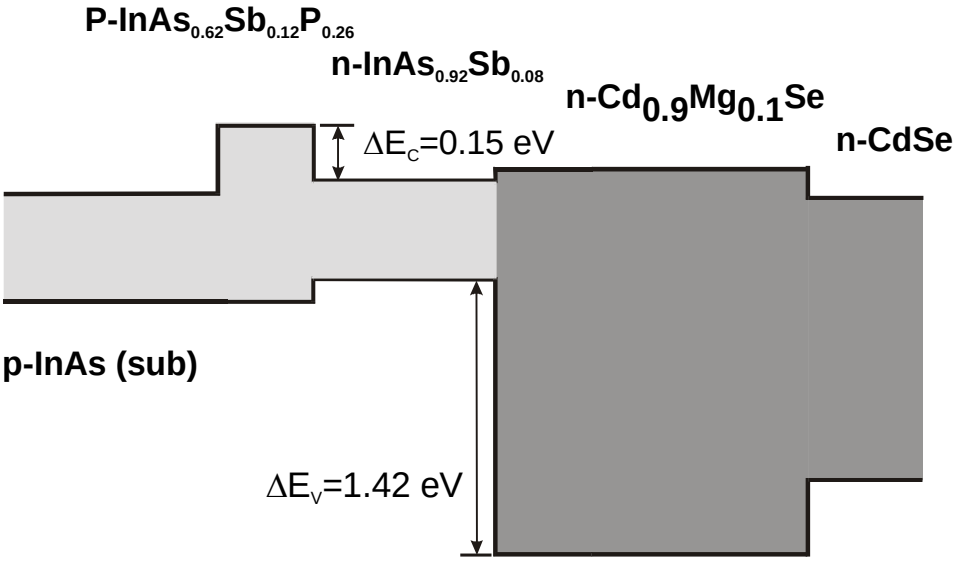

Fig.1.1 Schematic energy band diagram of the laser structure grown by hybrid epitaxial method.

1.2. Characterization of the laser structures and interface quality

The combine study of the surfaces of facet mirror of the hybrid p-InAs/p-InAsSbP/n-InAsSb/n-CdMgSe structure by Atomic force microscopy (AFM) and Electrostatic force microscopy (EFM) were undertaken at 300 K [20]. The AFM studies permitted to reveal the laser mirror surface topography and the EFM studies permitted to reveal surface potential distribution on the facet mirror. The EFM measurements of surface potential distribution on the laser mirrors make possible the finding of the epilayer sequence in the laser structure as well and, what is even more important, to establish the distributions of built-in and applied electric fields in the laser structure. The surface potential of the laser mirror surface in the location of each epilayer is determined by the combination of the work function value of the compound and the electric field distribution along the structure growth axis. In the EFM mode the difference of surface potentials of the probe and the sample materials is directly measured at the probe tip position on the surface (Kelvin probe force microscopy (KPFM) mode). The probe scanning over the sample surface in Kelvin mode allows obtaining the distribution of the potential in a plane of the surface under study, and, as well, along the laser growth axis. Recently, it was shown that performing KPFM measurements in a special AFM mode as Kelvin probe force gradient microscopy mode (KPFGM), when the electrostatic force gradient is detected, considerable improvements in the precision of voltage observations and measurements are obtained [21]. The KPFGM measurements allow completely avoiding the art-effects related with the protrusions and suppressions in surface topography. The phase shift (measured in degrees) of the EFM probe oscillation in the gradient of electrical field between surface and probe is detected. In our measurements one degree corresponds to a potential difference by 109 mV between the surface and the probe end.

In the KPFM potential topography image of the unbiased structure the all layers were distinctly found out (Fig.1.2a). The layer sequence corresponds to the contrast of the image (from the left to the right): p-InAs substrate, confining p-InAsSbP layer, p-InAsSb active region and confining n-CdMgSe layer, one after another. The weak contrast difference for the three first layers is due to various work functions of these compounds. The thickness of the InAsSbP and InAsSb layers was of 1.9 μm and 1.6 μm, respectively. The thickness of CdMgSe layer of 2 μm was found. Fig.1.2b demonstrates the KPFM surface potential profile obtained on the mirror of unbiased hybrid InAs/InAsSbP/InAsSb/CdMgSe laser structure. The surface potentials of substrate p-InAs and p-InAsSb layer are nearly the same that is reasonable since the Sb content in the epilayer is rather small. At the same time, surface potential for p-InAsSbP layer is higher by 60 mV. It means there could be found potential barriers on the left and right interfaces of that layer.

The appreciable increasing in surface potential was found at the p-InAsSb/n-CdMgSe heteroboundary that determines the position of the p-n junction in the structure. The potential difference by 280 mV in this place correlates with the expected value of the energy gap of the InAsSb layer (Eg=0.3 eV). A more accurate consideration revealed that the potential step actually consists of two steps of 90 mV and 180 mV separated by 0.2 μm. From that observation we may conclude that p/n junction does not totally coincide with the InAsSb/CdMgSe heterointerface due to some lack of uniformity in the II-VI part.

The additional confirmation of the localization of the p-n junction observed in the laser structure was found in Kelvin mode measurements under forward and reverse applied biases. Fig.1.3 presents surface potential profiles when structure was biased to n-contact with +0.1V and –0.1V, respectively. Comparison of the two potential profiles shows that the main part of applied bias drops on near the InAsSb/CdMgSe heterointerface. Moreover, it can be noticed that the change from –0.1V to +0.1V shifts the potential step a little to the left side. It means that the bias drop occurs preferentially on the left part of the potential step.

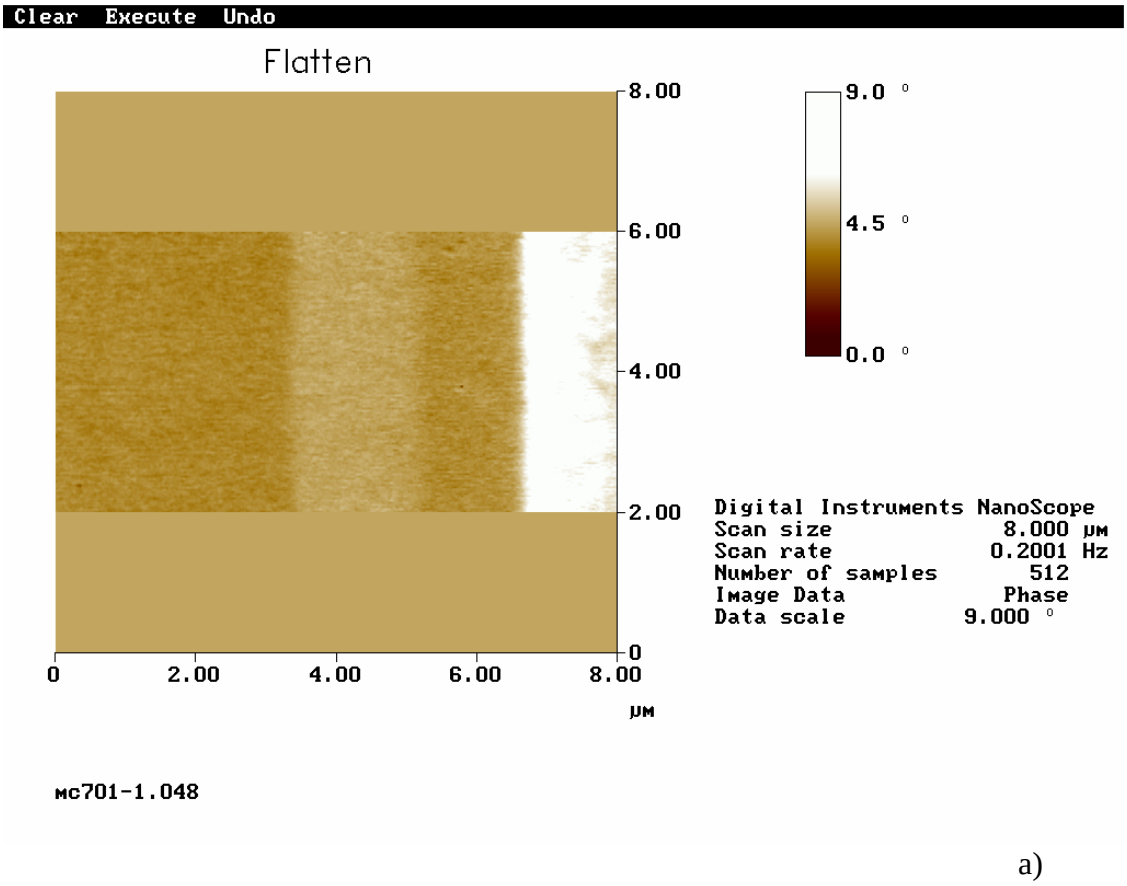

a)

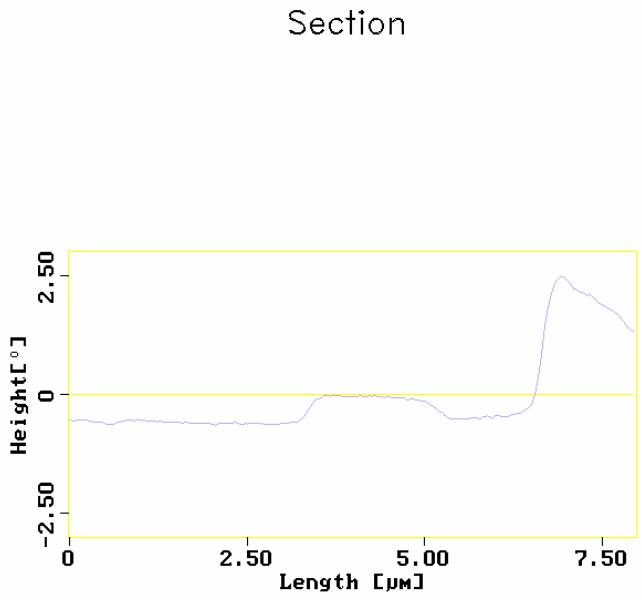

b)

Fig.1.2. KPFM surface potential topography (a) and KPFM potential profile (b) on the mirror of unbiased hybrid InAs/InAsSbP/InAsSb/CdMgSe laser structure.

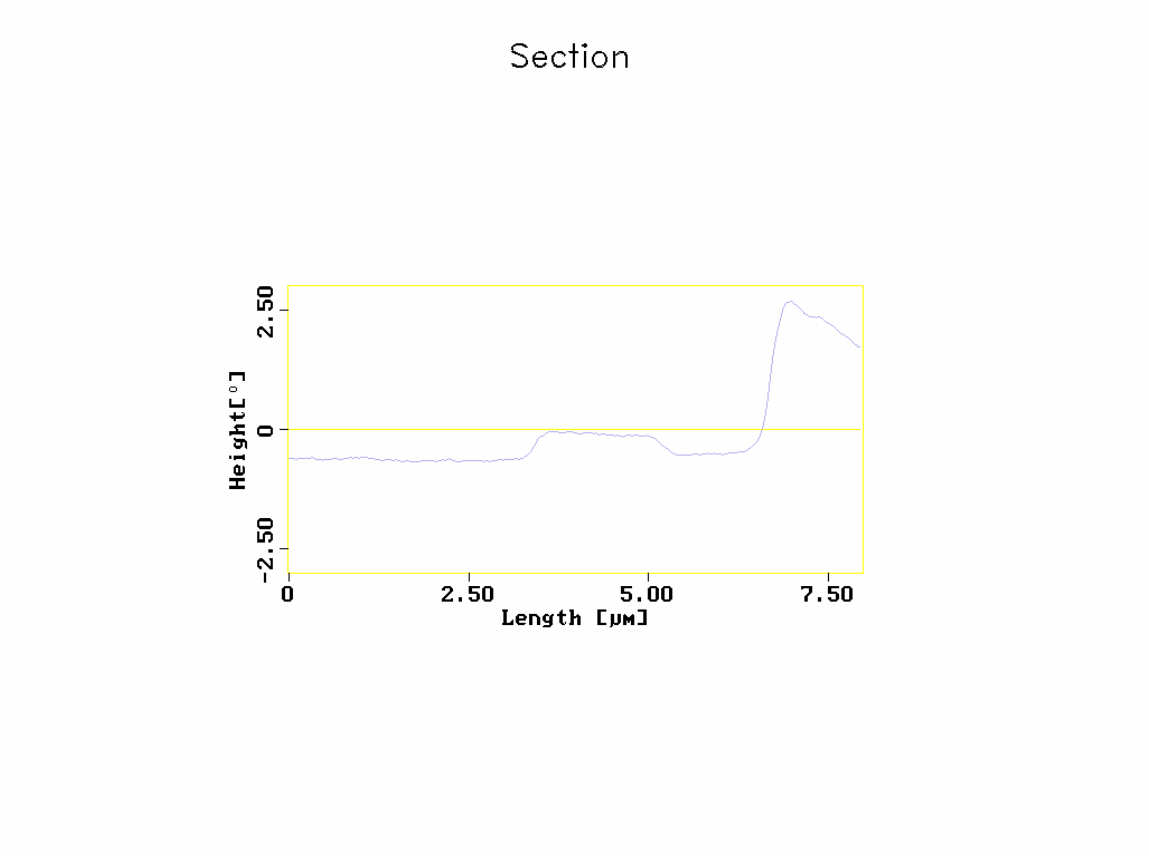

a)

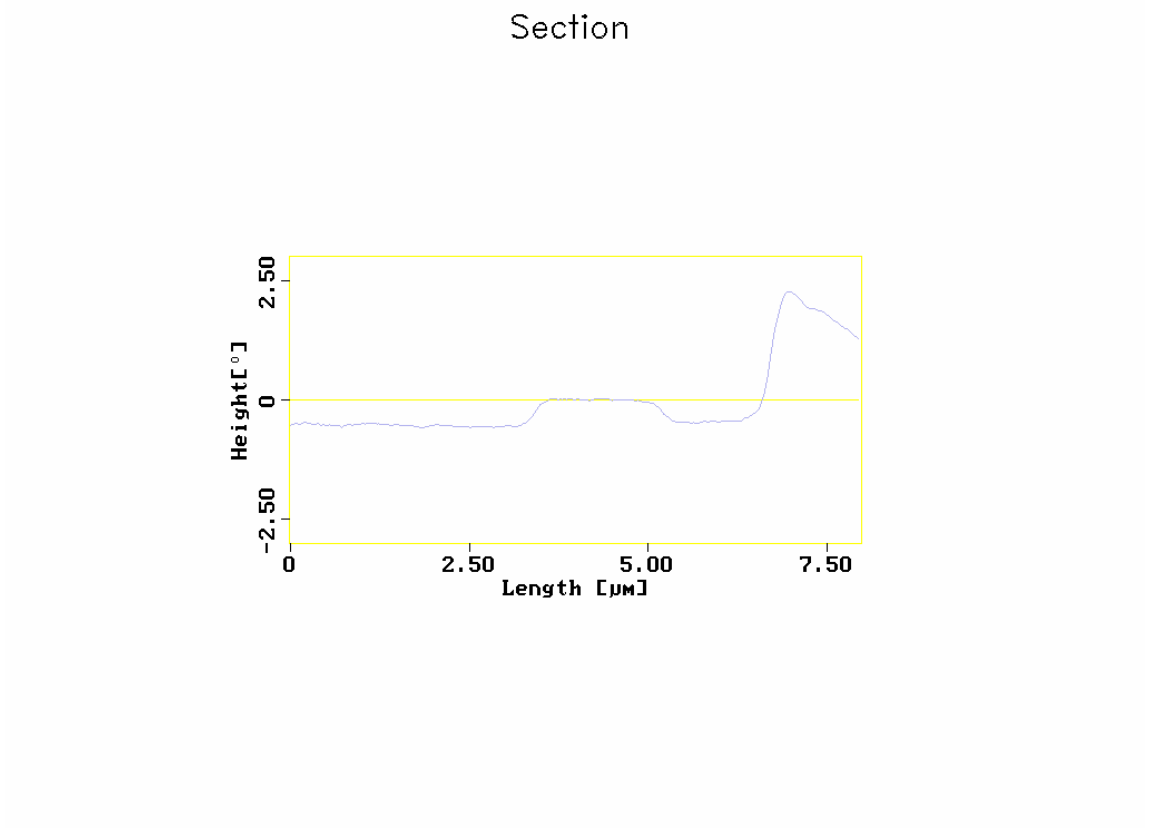

b)

Fig.1.3. KPFM potential profile under external bias: a) - 0.1V and b) +0.1V on the top n-CdMgSe layer

It should be also noticed that about 15% of the total applied bias appears at the p-InAsSbP/p-InAsSb interface. It means that there is a potential barrier between layers that causes a parasitic drop of the applied bias.

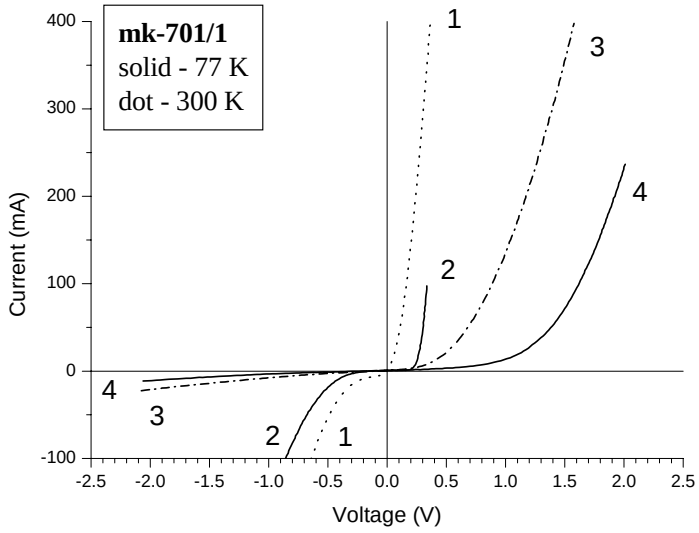

Fig.1.4. I-V characteristics of double InAsSbP/InAsSb/InAsSbP heterostructure (1,2) and hybrid InAs/InAsSbP/InAsSb/CdMgSe laser structure (3,4).

The *I-V* characteristics were measured independently for the p-InAs/P-InAsSbP/n-InAsSb basic heterostructure and the hybrid laser diode (Fig.1.4). Diode-like behavior of the *I-V* characteristics was obtained for both heterostructures. The direct curve cut-off voltage U~0.28 V at 77 K found for the basic structure is obviously determined by the forbidden gap of the InAsSb active layer. Employing the cladding *n*-CdMgSe layer instead the *n*-InAsSbP one in the laser structure leads to changing the design symmetry and improvement of *I-V* characteristics is observed. A polynomial-like dependence of direct *I-V* curve for the hybrid laser in contrary to the sharp turn on in the *I-V* characteristics of the III-V part only indicates that a significant series resistance has been introduced at the InAsSb/CdMgSe heterovalent interface.

1.3. Study of spontaneous and coherent emission

Electroluminescence (EL) study of the InAs/InAsSbP/InAsSb/CdMgSe laser structure was performed using a liquid-N_2 cooled InSb photodiode (EG&G Judson), 0.5-m monochromator (Digikrom Instruments) and SR810 Stanford lock-in amplifier for detecting the light emission from the sample. EL spectra were observed under both pulse regime and quasi steady-state conditions in the temperature range 77-300 K. Long-duration pulses (τ=1 ms) of driving current with the repetition rate of 500 Hz were applied.

Fig.1.5 presents EL spectra obtained for the asymmetric hybrid laser structure at 80 K. In the structure the spontaneous emission was observed starting with photon energy of about 0.337 eV that is smaller in energy of 14 meV than energy gap of the ternary $InAs_{0.92}Sb_{0.08}$ active region, which reveals broaden symmetric emission band (dotted line).

With the current increasing the EL spectra for the hybrid structure moved towards high energies by 20 meV and the spectra had asymmetric shape with sharp high-energy edge

and exponential long-wavelength tail (Fig.1.6). The EL peak behavior with increasing of the driving current is similar to that the radiative transitions occur due to filling the active region by electrons and holes from the cladding layers simultaneously. In this case luminescence appears as inter-quasi-Fermi levels recombination starting with conduction band-acceptor level transitions, which transformed to interband recombination with some Moss-Burnstein shift. Thus, we can conclude that the type II p-InAsSbP/n-CdMgSe heterojunction governs EL properties of the hybrid laser structure.

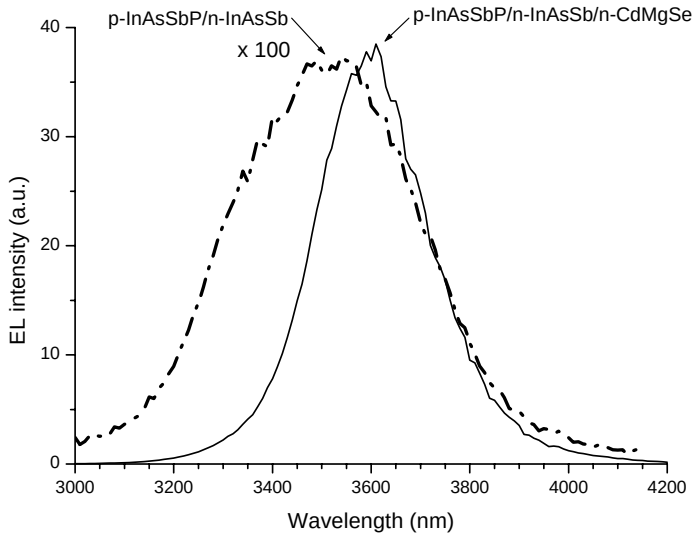

Fig.1.5. Spontaneous emission for the basic (III-V part only) structure and the hybrid laser structure at 80 K

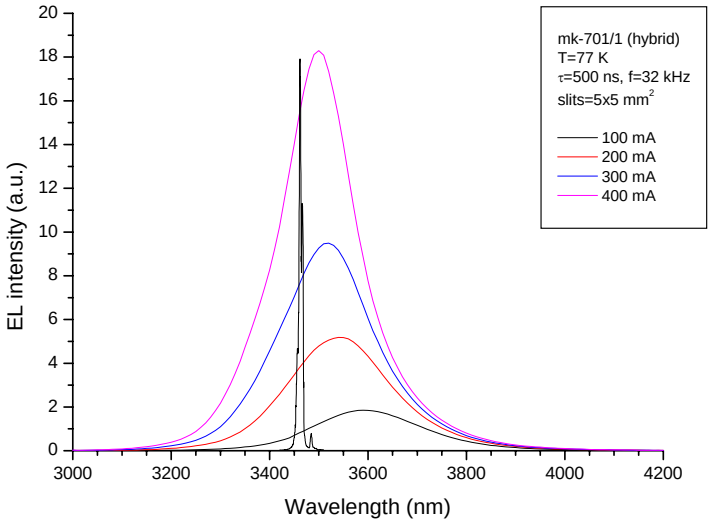

Fig.1.6. Spontaneous and coherent emission spectra for hybrid InAs/InAsSbP/InAsSb/CdMgSe laser structure.

The lasing at λ=3.5 μm was peaked at the high-energy side of EL spectrum and was related with interband radiative recombination transitions in the n-$InAs_{0.92}Sb_{0.08}$ active region. Coherent emission was achieved under high injection current conditions. In the best samples the threshold current density as low as J_{th}=4 kA/cm^2 was achieved at 80 K.

It should be noted that the hybrid InAsSbP/InAsSb/CdMgSe laser structure exhibited high-efficient output intensity of EL. It was detected the EL intensity exceeding by 2 times and up to 10 times the EL intensity in conventional InAsSbP/InAsSb/InAsSbP DH-laser structure grown by LPE and the hybrid AlGaSb/InAs/CdMgSe heterostructure grown by MBE only, reported elsewhere [12], respectively. It can be explained by the fact that the latter structure with adjacent layers of different isovalent compounds contains significant concentrations of mismatched defects at the active region heterointerface. That resulted in the external efficiency reduction.

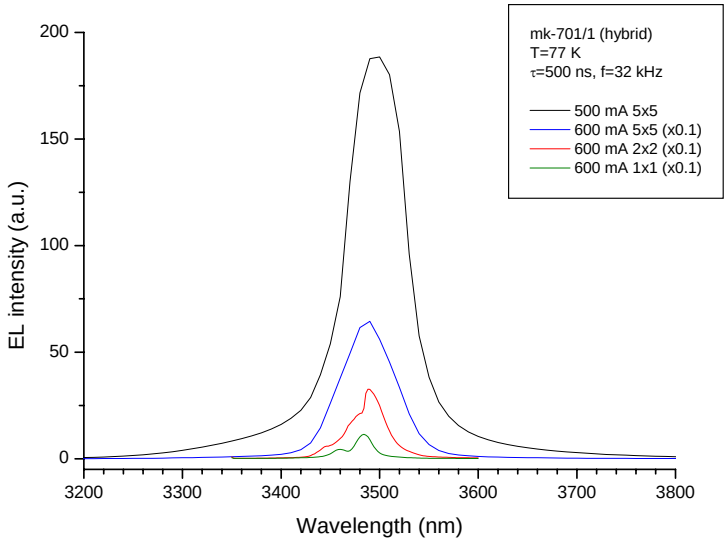

Fig.1.7. EL spectra for the hybrid InAsSbP/InAsSb/CdMgSe laser structure near the lasing threshold for various slits width.

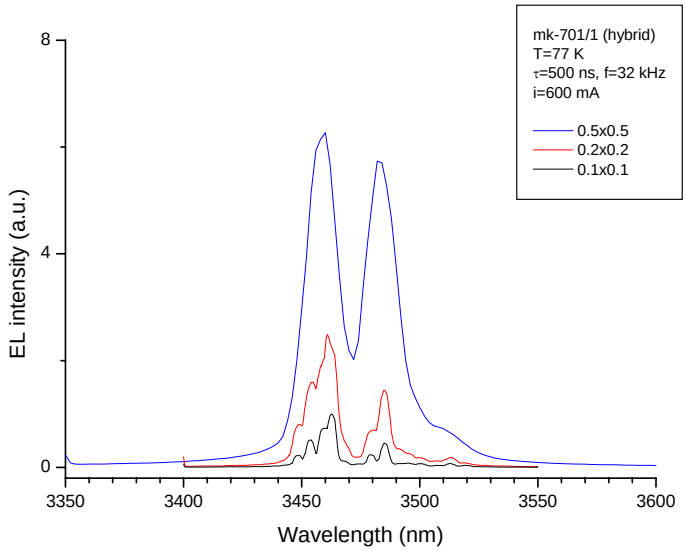

Fig.1.8. Coherent emission for the hybrid InAsSbP/InAsSb/CdMgSe laser structure beyond the threshold current for different slits width

Multi-mode coherent emission at 77 K was achieved under high injection currents (Fig.1.9). An average inter-mode distance is detected as 4 nm. Blue shift of lasing modes

towards to higher energy by 2 nm was observed with drive current increasing above the threshold value in the range from $1.1I_{th}$ to $1.6I_{th}$.

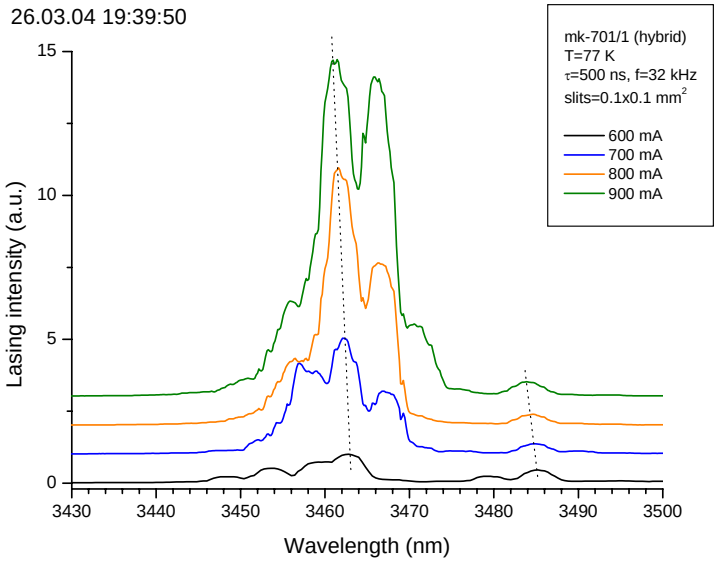

Fig.1.9. Blue shift of mode picture for the hybrid InAsSbP/InAsSb/CdMgSe laser structure with drive current increasing above the threshold

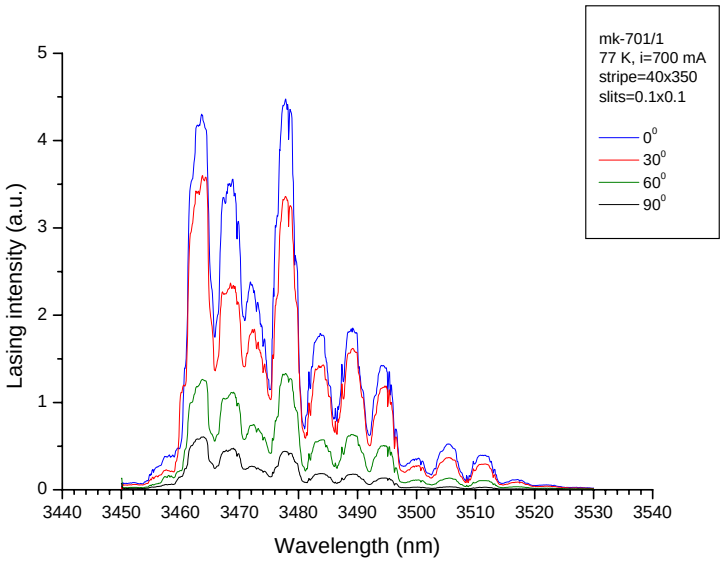

Fig.1.10. Polarization features of lasing spectra for the hybrid InAsSbP/InAsSb/CdMgSe laser structure

1.4. Optical confinement in the $CdMg_{0.1}Se/InAsSb_{0.08}/InAsSb_{0.13}P_{0.26}$ hybrid structure

In hybrid $CdMg_{0.1}Se/InAsSb_{0.08}/InAsSb_{0.13}P_{0.26}$ laser heterostructure there is a strong optical confinement of electromagnetic wave by $CdMg_{0.1}Se$ epilayer where permittivity (ε_c=6.5) is smaller by $\Delta\varepsilon$=5.89 than one of $InAsSb_{0.08}$ active region (ε_a=12.39) (Fig.1.11). In such layer a depth of the attenuation of coherent emission flow is about of 0.11 μm that is critically less than the thickness of the confining epilayer (2 μm) and the active region (1.6

μm). The sake of simplicity we consider that the coherent emission does not penetrate into $CdMg_{0.1}Se$ confining layer. On the other side the discontinuity of permittivity at the $InAsSb_{0.13}P_{0.26}/InAsSb_{0.08}$ heterointerface between the confining layer $InAsSb_{0.13}P_{0.26}$ (ε_c=12.04) and the active region is $\Delta\varepsilon$=0.35 only. Therefore, the penetration of lasing flow into that layer should be taken into account.

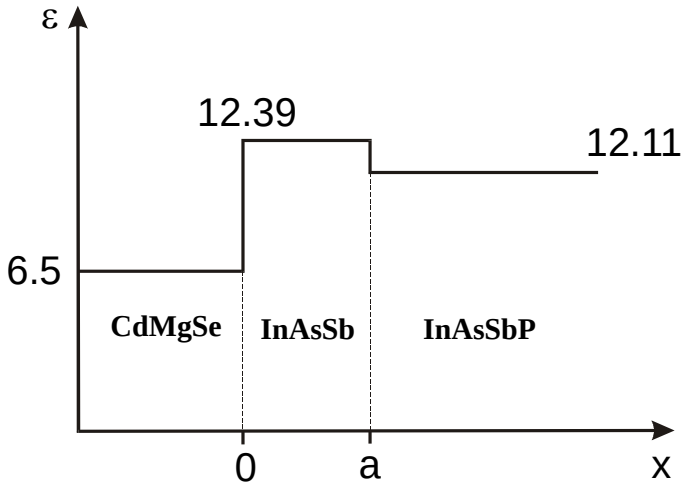

Fig.1.11. Distribution of permitivity in the hybrid laser structure

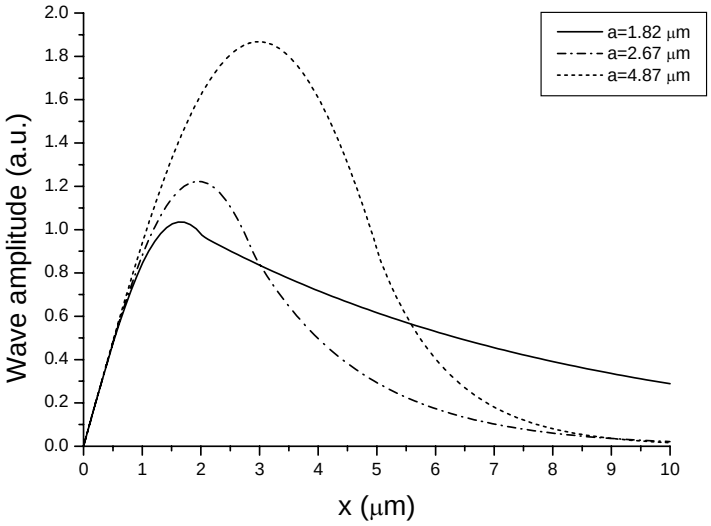

Fig.1.12. Distribution of lasing wave into the active region of the hybrid structure

Let's estimate the influence of minority carriers on the permittivity in the active region. The experimental data point out that the wavelength of a lasing mode (λ) decreases by 2nm with the increasing of drive current by 300 mA. Then, the changing of the permittivity with current increasing from zero to threshold value I_{th} can be expressed by formulae:

$$\Delta\varepsilon_{th} = \frac{2\varepsilon}{\lambda}\frac{d\lambda}{dI} I_{th}, \qquad (1)$$

where ε is permittivity for the wave propagation along the waveguide and it is intermediate magnitude between ε_a and ε_c. According with the equation (1) one can obtain $\Delta\varepsilon_{th}$=-0/024 at ε=12.2, λ=3.46 μm, I_{th}=500 mA и dλ/dI=-0.0067 μm/A. Although $\Delta\varepsilon_{th}$ can make worse the

optical confinement, we suppose that it is neglible due to the decreasing of ε_c caused by doping has the same order of magnitude.

Assumed simplification allows analytically to calculate a profile of the electromagnetic wave and a coefficient of the optical confinement (Γ) using Helmholtz wave equation for average amplitude of the wave (u) propagating in the direction of lasing mode:

$$\frac{d^2u}{dx^2} + (\frac{2\pi}{\lambda})^2(\varepsilon_x - \varepsilon)u = 0, \qquad (2)$$

where x is coordinate of thickness in the laser heterostructure (see Fig.1.11), ε_x is permittivity at the given coordinate. Origin of coordinates is placed at the InAsSb/CdMgSe heterointerface. Therefore, the InAsSb/InAsSbP heteroboundary of the active region is marked by a value of x=a. The solution of the equation (2) is following:

$u=A\sin(\alpha x) + B\cos(\alpha x)$, $\alpha=2\pi\lambda^{-1}k^{1/2}\Delta\varepsilon^{1/2}$ при $x\le d$ (3)

$u=e^{-\beta(x-a)}$, $\beta=2\pi\lambda^{-1}(1-k)^{1/2}\Delta\varepsilon^{1/2}$ при $x\ge d$ (4)

with boundary conditions:

at x=0 $u=0=B$ (5)

at x=a $u = A\sin\alpha a = \frac{\varepsilon_a}{\varepsilon_c}$, (6)

$$\frac{du}{dx} = \alpha A\cos\alpha a = -\beta\frac{\varepsilon_a}{\varepsilon_c} \qquad (7)$$

To calculate A the equation (7) should be divided by α and squaring, then it should be added up equation (6) which was squaring too. Finally, one can obtain

$$A = \frac{\varepsilon_a}{\varepsilon_c}\frac{1}{\sqrt{k}} \qquad (8)$$

Further, the equation for a(k) determination can be got from (7) and (8), but not from (6)

$$a = \frac{1}{2\pi\sqrt{\Delta\varepsilon}}\sqrt{k}\,\lambda\arccos(-\sqrt{1-k}) \qquad (9)$$

Thus, the profile of the lasing emission has sinusoidal shape into the active region of the laser and exponential shape into the pervious confining layer (Fig.1.12). As it is shown in Fig.2 the wave is sufficiently compact at average thickness of the active region in the range 2-3 μm (curve 2) whereas it penetrates deeply into confining layer at small thickness of the active region (curve 1) or it is localized and spreading into the wide active region (curve 3).

Optical confinement coefficient Γ is determined as a ratio of integral of emission intensity (u^2) on coordinate into the active region to total integral emission intensity:

$$\Gamma = [1+k^{3/2}(1-k)^{-1/2}\varepsilon_c^{\,2}\varepsilon_a^{-2}(\alpha a-0.5\sin2\alpha a)^{-1}]^{-1} \qquad (10)$$

The ratio of a/Γ is very important because it is proportional to threshold current density. The value of the ratio is minimal at a_{opt}=2.7 μm whereas it strongly rises with any deviation from optimal value and becomes infinite at a_{min}=1.635 μm (Fig.1.13). The penetration depth ($0.5\beta^{-1}$) of the lasing mode in the pervious confining layer decreases with the increasing of a. It is $0.5\beta^{-1}$=1 μm at optimal thickness of the active region.

At $a<a_{opt}$ the lasing mode penetrates into the InAs substrate and it can reach ohmic contact at $a=a_{min}$. The disappearance of confinement under the decreasing of the thickness of the confining layer is very interesting feature that is absent in a symmetric waveguide. Transverse modes of higher order have an advantage at $a<a_{min}$ due to the substrate is thicker than epitaxial structure (as a rule $h<<a$). The power of transverse waves is uniformly distributed along the whole epitaxial layer structure grown by LPE. Its coefficient of optical confinement is:

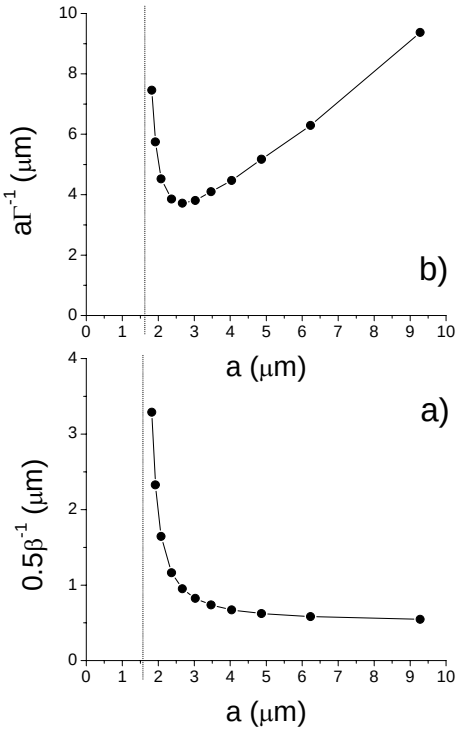

Fig.1.13. Dependence of penetration depth (a) and ratio a/Γ on the width of the active region

$$\Gamma = \frac{a}{h + a + l}, \qquad (11)$$

where l is a thickness of the pervious confining layer. Γ=0.01 at a=1.6 μm, h=150 μm and l=1.5 μm. Evidently, such magnitude of Γ is typical for most of longwavelength lasers. The obtained value of the ratio a/Γ is equal 150 that can be dicrease by 40 times with the improvement of the laser structure.

To compare the experimental data on the threshold current and the values theoretically calculated ones we assume that interband radiative recombination dominates

$$I_{th} = qLba\alpha_{\Sigma}\Gamma^{-1}\pi^{-3/2}c^{-2}\hbar^{-3}kTE_g^{\,2}\varepsilon(m_p/m_n)^{3/2}\exp(E_{F0}/kT), \qquad (12)$$

where q is the charge of an electron; L and b are the cavity length and the stripe width, respectively; α_{Σ} are total optical losses; E_{F0} is a quasi Fermi level in the conduction band at the inversion point. We have obtained the threshold current I_{th}=440 mA at following parameters: L=300 μm, b=40 μm, a=1.6 μm, α_{Σ}=50 cm^{-1}, Γ=0.01, E_g=0.33 eV, kT=0.0067 eV, m_p/m_n=20, ε=12.39 and E_{F0}=3kT. The computed value is in good agreement with the threshold current experimentally observed (I_{th}=500 mA).

2. Study of AlSb/InAsSb quantum well structure as an active region of the lasers for the spectral range 3-4 μm.

The AlSb/InAsSb/AlSb quantum wells as an active region of the injection lasers for the spectral range 3-4 μm were grown by MOVPE method on GaSb substrate. Characterization of their heterostructures, investigation of electroluminescent properties, as well as theoretical calculation of radiative recombination transition and an estimation of threshold current density depending on quantum well width were performed.

2.1. Characterization of InAsSb solid solutions grown by MOVPE method

The structures under study were grown on InAs and GaSb (100) oriented substrate in an AIXTRON 200 machine with RF heated graphite susceptor in horizontal reactor by low-pressure MOVPE. In order to check electrical quality of the narrow-gap InAsSb epilayers there was used semi-insulating InAs substrate heavily compensated with Mn to hole concentration 1×10^{17} cm^{-3} at 300 K. Hall measurements carried out on a single n-InAsSb/p-InAs:Mn heterostructure based on ternary undoped epilayer revealed electron mobility of 38000 $cm^2/V*s$ and carrier concentration of $n=2.6\times10^{16}$ cm^{-3} at 77 K for Sb=0.08 in solid phase, whereas the decreasing of Hall mobility down to 5000 $cm^2/V*s$ for Sb=0.22 was observed. Mesa etching of the wafer structures for EL measurements and Ohmic contacts were performed using standard photolithography alignment system and vacuum sputtering set-up.

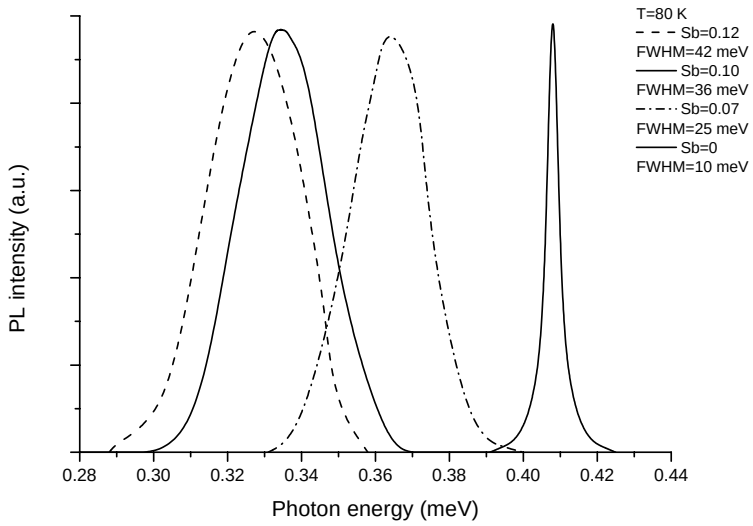

Fig.2.1. PL spectra at 80 K for undoped InAsSb epilayer of various compositions

Fig.2.1 presents photoluminescence spectra for undoped InAsSb epilayer of various compositions measured at 80 K. It should be noted that intensity of PL peaks decreased with Sb increasing in solid solution and the emission bands become broaden. The spectral position of maximum of the emission band for InAsSb solid solutions summarised in Table 1.

Table 1 PL characterization of InAsSb epilayers

Sample	Sb content in solid	Photon energy in maximum of PL at 80 K (eV)	FWHM (eV)
1	0	0.408	0.010
2	0.07	0.365	0.025
3	0.10	0.330	0.036
4	0.12	0.324	0.042

Electroluminescence spectra of InAs/InAsSb single heterostructure at 77 and 300 K are presented in Fig.2.2. For the undoped InAsSb epilayer EL spectra at 77 K contained two pronounced emission bands with photon energy at maximum $h\nu_L=0.352$ eV and $h\nu_S=0.408$ eV and FWHM of 23 meV. At room temperature EL spectra also contained two separate

emission bands with photon energy at maximum $h\nu_L$=0.306 eV and $h\nu_S$=0.357 eV but the peaks became wider and $FWHM_L$=40 meV and $FWHM_S$=60 meV were found. Some saturation for $h\nu_L$ peak intensity was observed. We have marked the peaks by L and S to indicate the signal from the epilayer and the InAs substrate, respectively. The energy shift of about 50 meV with temperature changing from 77 K to 300 K is close to the value observed for the InAs based materials. Using the calculation for unstrained epilayer based on the ternary $InAs_{1-x}Sb_x$ solid solution with antimony content of x=0.08 we have computed the energy of the forbidden gap of E_g=0.348 eV at T=77 K. 50 meV energy shift is visible with temperature increase from 77 to 300 K.

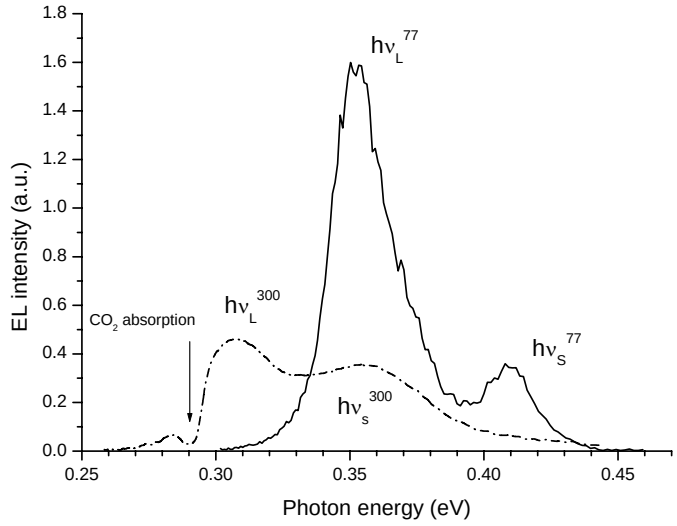

Fig.2.2. EL spectra measured for n-$InAs_{0.89}Sb_{0.11}$/p-InAs heterostructure at 77 K (solid line) and 300 K (dashed line).

2.2. Growing by MOVPE and characterization of AlSb/InAsSb quantum wells

Single and triple quantum well structures based on AlSb/InAsSb heterojunctions were grown by MOVPE. This epitaxial structure is a symmetric heterostructure with respect to p- and n-GaSb cladding layers sandwiching the active region consisting of single p-AlSb/n-$InAs_{0.89}Sb_{0.11}$/p-AlSb quantum well with the thickness of 10 nm and 6 nm for the barrier and the quantum well, respectively (Fig.2.3).

Atomic force microscopy investigations of the facial nanorelief of the cleavage surface of the GaSb/AlSb/InAsSb/AlSb/GaSb QW heterostructures were carried out, as well as surface potential distributions were studied. AFM topography data revealed the location of the structure interfaces on the cleavages. Topography relief image of the sample 1322A is shown in Fig.2.4a. A cross-section along the white line in the topography image is presented in Fig.2.4b. There is a 10-nm high step at the substrate-epitaxial layer heteroboundary that was formed during the cleavage procedure. The position of the AlSb/InAsSb/AlSb quantum well marked by the arrow coincides with the region of the crack. Similar morphology of the cleavage relief was also observed for the sample 1325A that contained triple AlSb/InAsSb/AlSb quantum well sandwiched by GaSb epilayers. The origin of such relief on the sample cleavages requires additional studying.

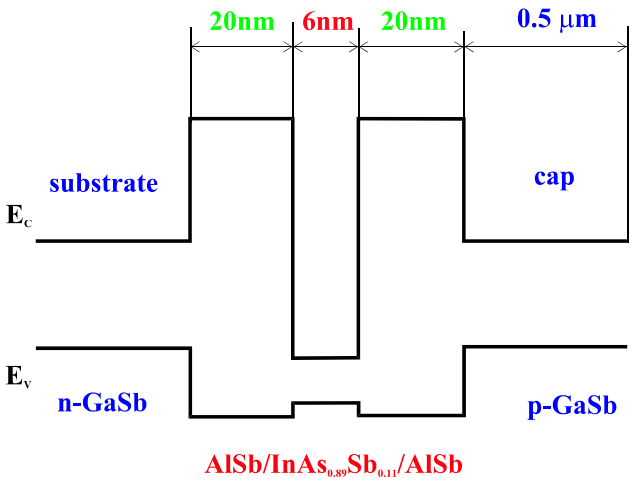

Fig.2.3. Schematic energy band diagram of single AlSb/$InAs_{0.89}Sb_{0.11}$/AlSb quantum well heterostructure

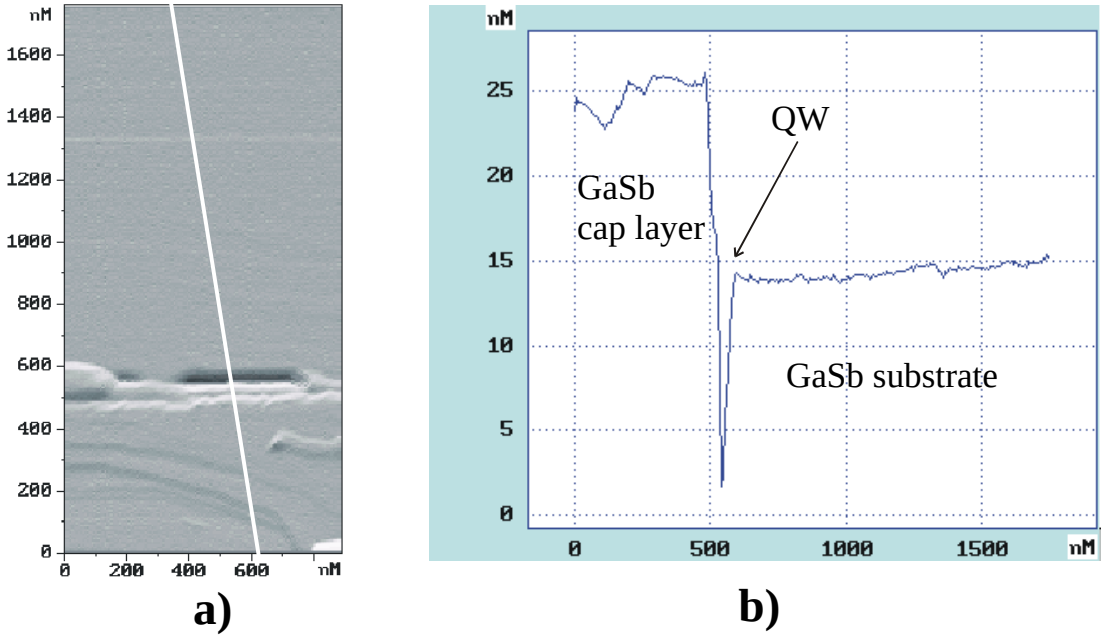

Fig.2.4. AFM topography image (resonant mode, NSG11/Pt probe) and a cross-section along the white line in the image.

To evaluate the width and the location of the p-n junctions along the structures, the scanning Kelvin probe microscopy (SKPM) was applied. The variations of the bulk potentials due to external bias are rigidly bound with the changes of surface potentials potential that can be traced by SKPM. It can be done by the measurement of surface voltage drop (SVD) profile [20]. The SVD is a difference between the contact potential drop (CPD) measured under external bias and CPD measured at earthed terminals, respectively. Usually, the SVD depends on an external bias linearly although its value differs from the actual applied bias on experiment. It can be ascribed to the influence of instrumental effects that can be taken into account [21]. When the relation SVD - applied voltage is nonlinear the correction of SVD due to instrumental contribution becomes ineffective. That nonlinear relation and a strong deviation of the SVD from the real voltage drop mean that the requirement of the subsurface band bending invariability is disturbed. In fact, these deviations of the subsurface band banding and, hence, the surface potentials can be associated with the flow of nonequilibrium

minority carriers towards the surface. These minority carriers can be injected, for example, across the p-n junction.

Fig.2.5 shows the results of the SKPM study of the sample under study. The data were obtained for various forward and reversed bias applied to the structure. When p-n junction is closed (small bias) the linear relation of SVD value on the applied voltage (see Figs 2.5a,d). The increase in the forward bias leads to the asymmetry in SVD profile due to the rise of drive current owing to the p-n junction becomes open.

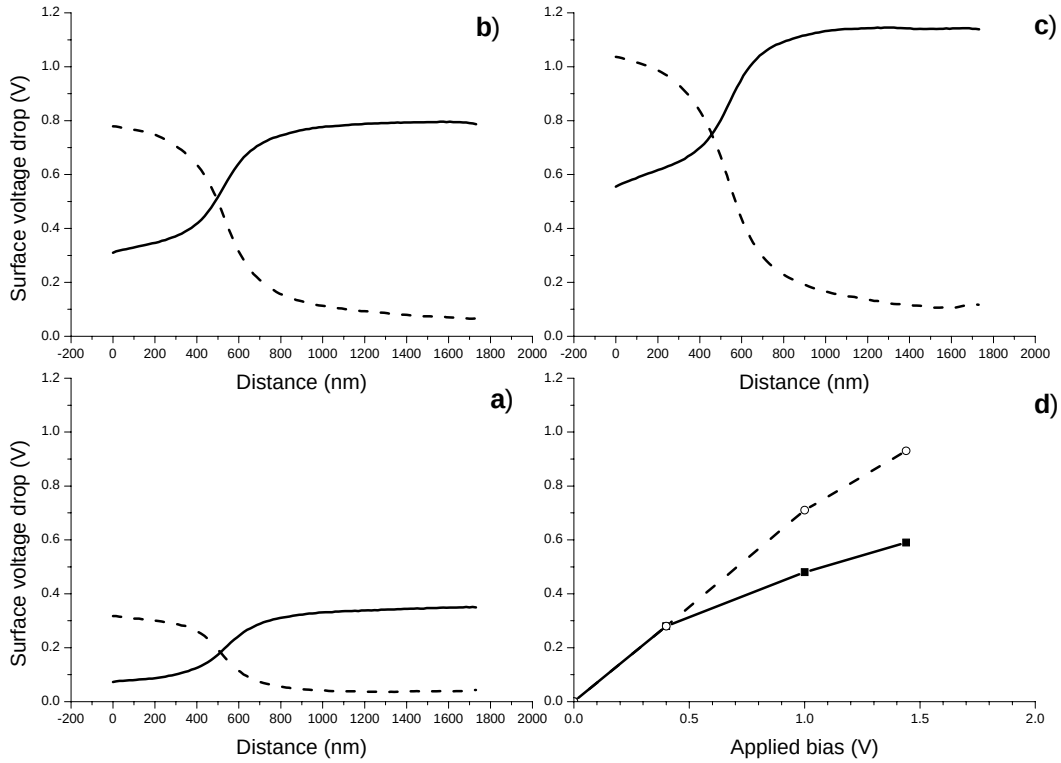

Fig.2.5. KPFM (lift mode) study of the redistribution of surface voltage drop (SVD) profiles for different bias: 0.4V (a), 1.0V(b), 1.44V(c), d) -Comparison of SVD value at the given bias. The SVD profiles under forward and reversed applied bias are shown by solid and dashed line, respectively.

The pronounced difference in SVD for forward and reversed bias can be explained by a large change of the subsurface band bending at the cleaved facet of the structure due to strong surge of the minority carriers from the quantum well. However, the direct improvement of that can be obtained during the study of the distribution of the surface potential under illumination.

2.3. Study of spontaneous emission of the AlSb/InAsSb/AlSb quantum well

The GaSb/AlSb/InAsSb/AlSb/GaSb QW structure revealed a strong rectifying I-V characteristic and its weak dependence on temperature in the range from 77 K to 300 K under both forward and reverse bias was observed (Fig.2.6).

An intense EL for the GaSb/AlSb/InAsSb/AlSb/GaSb QW heterostructure was observed at 77 K in the spectral range 0.3-0.4 eV and it revealed single pronounced emission

band at $h\nu^{77}$=0.360 eV (Fig.2.7). The average value of FWHM was estimated to be 23 meV. At room temperature two EL peaks with photon energy at maximum $h\nu_1^{300}$=0.324 eV and $h\nu_2^{300}$=0.344 eV were found (Fig.2.8). The FWHM of the first peak was about 26 meV while the second peak had sharp high-energy edge and FWHM of 11 meV computed from Gassian deconvolution. The EL intensity at room temperature was ten times lower than one at low temperature. The EL intensity increases with increasing current injection while the spectral position of EL peaks remains unchanged at both temperatures.

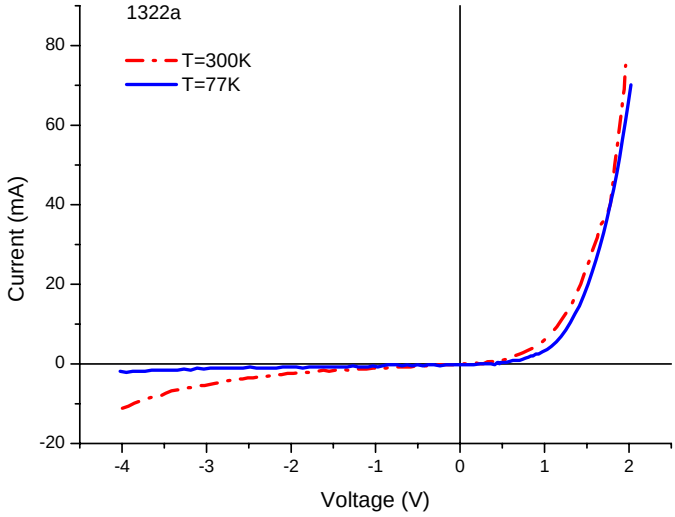

Fig.2.6. I-V characteristics measured for single QW AlSb/InAsSb/AlSb heterostructure at 77 K and 300 K.

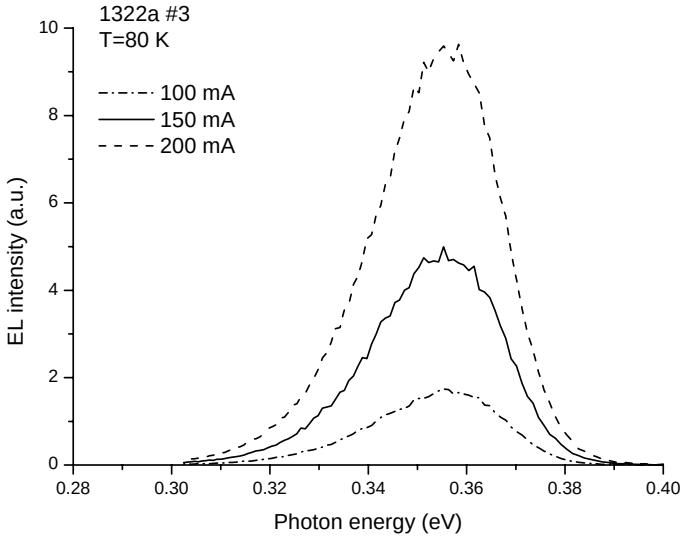

Fig.2.7. Evolution of the EL spectra measured for single AlSb/InAsSb/AlSb QW heterostructure at 80 K

The obtained values of photon energy of emission bands exceeded the energy gap of the ternary solid solution. So, we can conclude that radiative transitions take place in the AlSb/InAsSb/AlSb quantum well. The energy spectrum of the QW under study was theoretically estimated. The radiative recombination occurs from the lowest electron level in the QW to the hole states near the top of the valence band. The EL intensity increases with

increasing current injection while the spectral position of EL peaks remains unchanged at both temperatures.

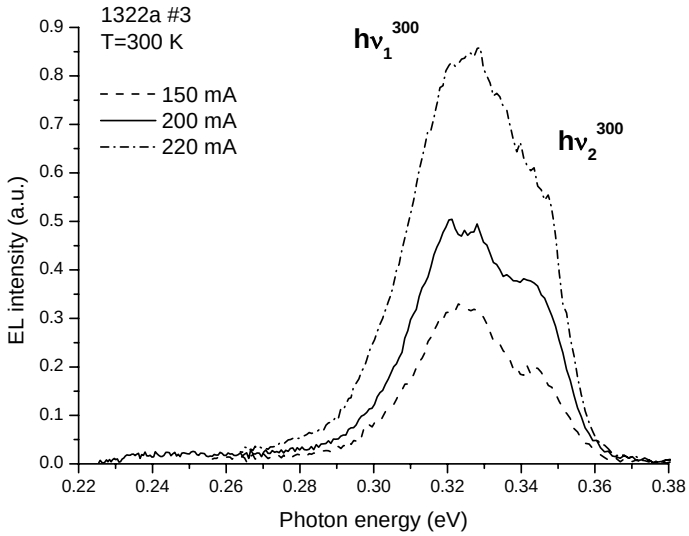

Fig.2.8. Evolution of the EL spectra measured for single AlSb/InAsSb/AlSb QW heterostructure at 300 K.

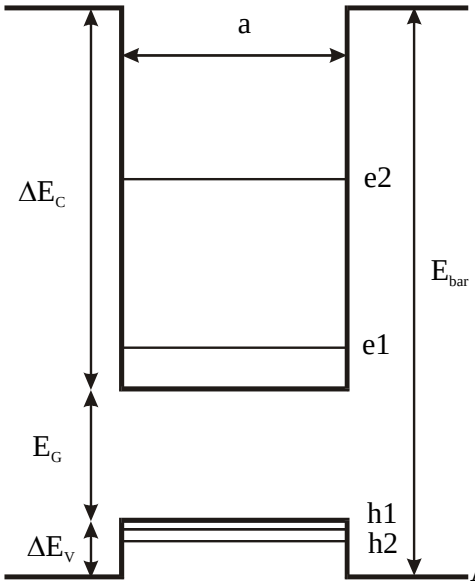

According our calculation for electrons and holes localized in the narrow-gap active layer the QW has two electron subbands, at least, and a few holes levels (Fig.2.9). We suppose that the radiative transitions at low temperature (77 K) occur between the ground electron and hole space-quantization levels with the photon energy exceeded the energy gap of ternary InAsSb solid solution. The carrier (electron and hole) concentration is expected to increase with the rise of operating temperature from 77 K to 300 K under fixed injection level. Following this, two emission bands were observed in the EL spectra at 300 K. The spectral positions of the emission bands still remain with driving current. These EL peaks can be ascribed to radiative transitions into the QW between the ground electron level and two occupied hole levels, respectively. Due to strong hole localization the FWHM of the emission band was found to be in twice smaller (15 meV) than one for the 3D semiconductor.

The space quantization spectrum of electrons and holes in a single type I quantum well was calculated in the frame of the four-band Kane's model taking into account intermixing of s- and p-states [2]. The photon energy of radiative recombination transitions of

charge carriers considering Coulomb interaction of localized electrons and holes were computed for 77 K and 300 K. It was demonstrated that Coulomb interaction essentially determines the value of the energy shift of emission band maximum. In this case, with increasing temperature the emission maximum of the EL peak moves to the longwavelength side less than it was expected for bulk semiconductor. The calculated values of ground recombination transitions obtained for 10nm thick QW ($h\nu_1^{300}$=0.329 eV and $h\nu^{77}$=0.368 eV) are in good agreement with experimental data. The mechanism defining the broadening of emission bands was analyzed. It was shown that main contribution in the spectral line broadening is the hole-hole scattering. Characteristic time of the scattering is about of 10^{-12} s at 77 K while this time increases by an order for 300 K.

2.4. Theoretical computation of radiative and non-radiative recombination in asymmetric quantum well

Total threshold current density for wavelength lasers mainly consists of the contribution of radiative and non-radiative Auger recombination currents: $J_{th} = J_{th}^{R} + J_{th}^{A}$. There is different dependence of each of these currents on quantum well (QW) parameters (width of the well, barrier height etc).

Threshold current density for radiative recombination transitions in a quantum well is

$J_{th}^{R} = e \cdot N_{QW} \cdot B^{2D} \cdot n_{th}^{2D} \cdot p_{th}^{2D}$,

where e- electron charge, N_{QW}- number of QWs, B^{2D}- radiative recombination constant, n_{th}^{2D} and p_{th}^{2D}- threshold concentration for electrons and holes, respectively, at that $B^{2D} \sim 1/T$ and $n_{th}^{2D}(p_{th}^{2D}) \sim T$. Therefore, radiative current is $J_{th}^{R} \sim T$ and it weakly depends on width and depth of the quantum well.

The dependence on the width of the quantum well is determined by the integral of electron and hole wave function overlapping

$$|I_{CV}|^2 = \left| \int_{-\infty}^{+\infty} \psi_C(x)\psi_V(x)dx \right|^2 ,$$

where $\psi_C(x)$ and $\psi_V(x)$ are wave functions for electrons and holes, respectively.

Auger-recombination current in QW can look like

$$J_{th}^{A} = eN_{QW}[C_{CHCC}^{2D} n^2 p + C_{CHHS}^{2D} np^2] ,$$

where C_{CHCC}^{2D} - Auger coefficient ascribed to transitions of an electron to excited state, C_{CHHS}^{2D} - coefficient ascribed to transitions of a hole to spin-splitted band and total Auger coefficient is $C^{2D} = C_{CHCC}^{2D} + C_{CHHS}^{2D}$.

The dependence of the total Auger coefficient on the QW width is non-monotonic function and it is sufficiently determined by the overlapping integral of carrier's involed in the radiative recombination. The overlapping into the QW is small for thin well due to a wave function penetrate through the barrier. The increasing QW width leads to the increasing of Auger coefficient value. However, under some width of the QW a magnitude of the overlapping is saturated and then Auger coefficient decrease owing to the localization region becomes lower.

The results demonstrated in this report allow considering the quantum well AlSb/InAsSb/AlSb heterostructures grown by MOVPE as promising materials to design of mid-infrared laser diodes operating in 3-4 μm with advanced emission performance at high temperatures.

3. Study of wide-gap cladding layers for asymmetric laser structure.

3.1. Growing of InAsSbP layers with maximum content of phosphorus (P<60%) by MOCVD method.

The main attention in the quarter III of the project was paid to growing and study of wide-gap cladding layers for asymmetric laser structure: the growing of InAsSbP layers with maximum content of phosphorus (P>50%) by MOCVD on InAs substrates.

$InAs_{1-x-y}Sb_yP_x$ epilayes lattice-matched with InAs substrate were obtained by MOCVD both in the region of existence of solid solutions ($0<x<0.39$) and in the region of miscibility gap ($0.39<x<0.5$) [23]. The epilayers had mirror-like surface at phosphorus content near the 50%. The layer composition and mismatch was controlled by X-Ray mass spectroscopy method and double-crystal x-ray diffraction using the (004) reflection of Cu$K_{\alpha 1}$ radiation (Fig.3.1).

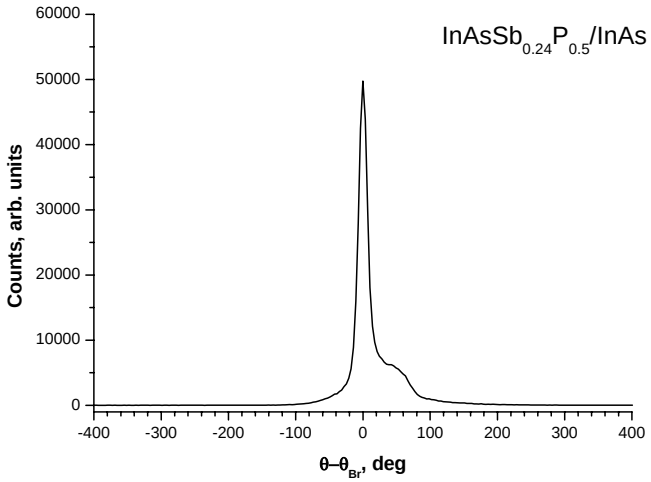

Fig.3.1. The lattice mismatch curve for the InAs/$InAsSb_{0.24}P_{0.5}$ heterostructure obtained by double-crystal x-ray diffraction using the (004) reflection of Cu$K_{\alpha 1}$ radiation.

To estimate an efficiency of electron confinement, InAsSbP/InAs(Sb)/InAsSbP double heterostructures (DH) with wide-gap cladding layers (P=0.5, E_G=0.57 eV at 77 K) were grown on p-InAs substrate heavy doped with Zn by MOVPE and electroluminescence was studied. The structures were obtained in a horizontal reactor with RF heated graphite susceptor at atmospheric pressure. This epitaxial structure is a symmetric heterostructure with respect to p- and n-InAsSbP cladding layers sandwiching the 0.8-μm InAs active region with the thickness of 2 μm for the barriers.

The double-channel post-growth treatment of the obtained structures was performed using standard wet etching and Si_3N_4 covering (Fig.3.2)

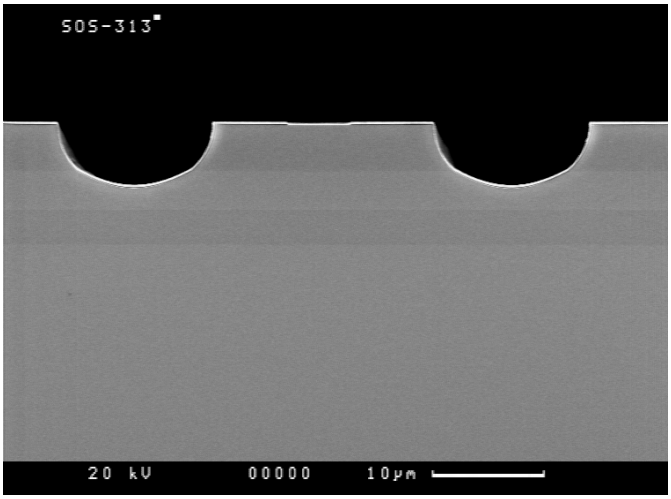

Fig.2. SEM photograph of the cleaved cross-section for InAsSbP/InAsSb/InAsSbP double heterostructure.

It was established that quantum efficiency of EL for light-emitting diodes based on wide-gap $InAsSb_yP_x$ epilayers with x=0.5 was to be higher in 2.5 times than for the structures containing cladding layers with low phosphorus content x=0.32 (Fig.3.3).

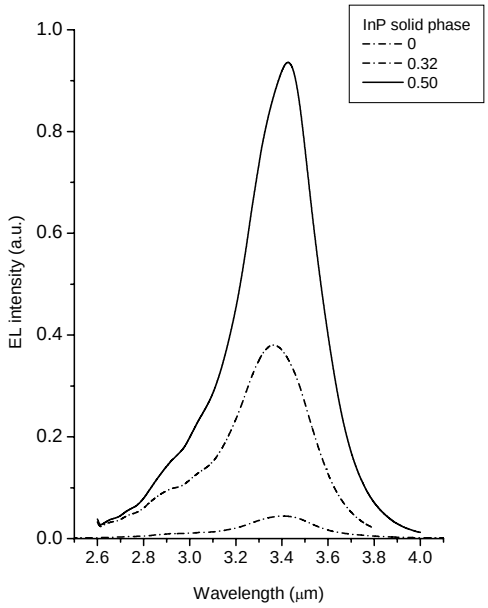

Fig.3.3 EL spectra at 80 K for symmetric InAsSbP/InAsSb/InAsSbP DH for various P content in confining layers.

Coherent emission peaked at 3.1 μm was achieved at the threshold current density as low as 150 A/cm^2 at 77 K. The lasing appeared in a maximum of the spontaneous spectra. This result is an evidence of good quality of wide-gap epilayers high phosphorus content grown by MOCVD and obtained in miscibility gap for regular InAsSbP solid solutions.

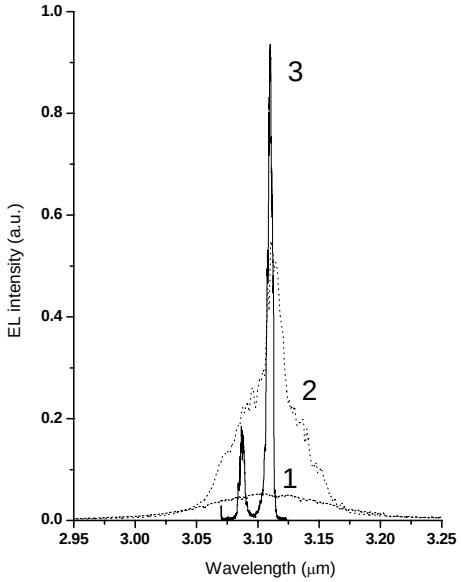

Fig.3.4. Spontaneous and coherent emission for InAsSbP/InAs/InAsSbP DH with P=0.50 in cladding layers.

3.2. Growing of AlGaAsSb epilayers by MBE method

The second task in the framework of the work plan of the project was determination of the optimal growth conditions of the wide-gap quaternary AlGaAsSb solid solutions obtained on InAs substrate by MBE. There are some technology problems due to the difference in chemical activity of the V group elements (As and Sb) the optimal MBE growth conditions depends on those elements content in the solid solution. It was shown that at the typical MBE growth rate V~1ML/s the substrate temperature regions, where the growth rate was limited by group V elements, are different and this difference was found to be ~100^0C between InAs and GaSb substrates.

An influence of the substrate temperate and value of the V group elements flux on composition, growth rate and quality of the AlGaAsSb epitaxial layers was investigated. For this purpose AlGaAsSb epitaxial layers at different fluxes of the As and Sb and substrate temperature in range of 460-550C were grown by MBE set-up DCA-350. Monitoring of the surface condition was carried out by RHEED. Composition of the solid solutions was determined with assistance of the micro X-Ray analyzer CAMEBAX and also by combination-crystal X-ray spectrometry methods. Microanalysis data of the metal components composition were used during the modeling and analysis of the X-Ray diffraction rocking curves for the more precise determination of the lattice parameter mismatch of the epitaxial layer and substrate.

It was established that the optimal substrate temperature for MBE growth of the AlGaAsSb solid solutions lattice-matched with InAs is 500-520 C. At higher temperatures the significant deterioration of the growth surface takes place. Increasing in the As and Sb fluxes to maintenance the stoihiometry on the growth surface initiates worsening of the structural quality of the AlGaAsSb epitaxial layers (intensity decrease on the X-Ray rocking curves and the peaks broadening were observed). Decrease of the substrate temperature lower than 470 C at the constant As and Sb fluxes leads to the significant lowering of the As content in epitaxial layers.

Substrate temperature and V/III flux ratio optimal for the epitaxial growth of the $AlGaAs_{0.09}Sb_{0.91}$ which has the same lattice constant with InAs turned out to be 515^0C and 1, respectively. At this temperature range Sb sticking coefficient depends on temperature weakly and no needs to use large antimonide flux to provide Sb-stabilized growth. At the same time to realize 10% As in the solid solution is necessary to have a low flux of the As. X-Ray diffraction curves of the $AlGaAs_{0.09}Sb_{0.91}$ grown at the optimal growth conditions contains one peak practically coincident with the peak of the InAs substrate with the same intensity.

Structures containing one and two quantum wells for EL study were grown on (100) *p*-InAs substrates by MBE with arsenic valved cracker cell. The typical structure consists of *p*-InAs buffer layer, 6 nm n-$InAs_{0.92}Sb_{0.08}$ quantum well surrounded by two 20 nm $Al_{0.5}Ga_{0.5}As_{0.08}Sb_{0.92}$ (*p* and *n* – doped, respectively) barriers and top *n*-GaSb contact layer. The second structure has the same buffer, barrier and contact layers but two 6 nm $InAs_{0.92}Sb_{0.08}$ (*p* and *n* – doped correspondingly) quantum wells in the active region separated by 4 nm *p*-$In_{0.1}Ga_{0.9}Sb$ barrier. The *n* region was doped with Si to 1×10^{18} cm^{-3} and the *p* region was doped with Be to 2×10^{19} cm^{-3}. In these structures, all active regions were grown at 430 ^{0}C and no spinodal decomposition process has been found from x-ray rocking curves.

Basic growth conditions for the InAs, AlGaSb, $InAs_xSb_{1-x}$ solid solutions by MBE were developed. Growth of the InAs was realized in substrate temperature range of 470^0-500^0C, surface smoothness and III/V flux ration were controlled “in-situ” by the RHEED. Optimal stoichiometry of the components was achieved at the surface reconstruction 3×1. Growth process in those conditions allows to achieve the typical value of the carrier mobility μ~10000 cm^2/Vs with electron concentration n~3.5×10^{16} $см^{-3}$. Narrow PL peak with FWHM=12 meV confirms a good quality of the surface. AFM investigations show that the average surface smoothness was as rough as < 0.5 nm. Valved Cracker cell VAC 500 was used as an As source for the growth of the $InAs_xSb_{1-x}$ That allows controlling the composition of V group elements with a high accuracy.

The results demonstrated in this report allow considering the wide-gap AlGaAsSb and InAsSbP epilayer grown by MOVPE as promising materials to design the confining layers of mid-infrared laser diodes operating in 3-4 μm with advanced emission performance at high temperatures.

4. Fabrication of InAsSbP/InAsSb/AlAsSb laser heterostructures growing by combine MOCVD technology method

4.1. Growing of n-InAsSbP/n-InAsSb/p-AlAsSb asymmetric heterostructures

The hybrid InAsSbP/n-InAsSb/p-AlAsSb laser structures were obtained by combine method using two separate epitaxial MOCVD growth setups for phosphorus-rich and aluminum-rich part, respectively. The heterostructures was grown on a n^+-InAs(100) substrate doped with S with carrier concentration n>$8\times10^{18}$$cm^{-3}$. The structure A consisted of the 2 μm-thick wide-gap n-$InAs_{1-y-x}Sb_yP_x$ cladding layer with high InP content in the range 0.4<x<0.5 and x/y=2.08, then 0.6 μm-thick narrow-gap n^0-$InAs_{0.92}Sb_{0.08}$ active region (E_G=0.347 eV at 77 K), then 0.8 μm-thick wide-gap p-$AlAs_{0.13}Sb_{0.87}$ cladding layer which were unintentionally doped, respectively. The 0.6 μm-thick p-GaSb cap layer was used on the top of the structure to prevent the oxidation of the Al-containing epilayer. As a result, the InAsSbP and AlAsSb cladding layers forming type II heterojunction between them confine electrons and holes in the active region of the structure under study due to asymmetric band-

offsets at the heteroboundary with the InAsSb active layer (Fig.4.1). The structure B differs from the structure A in a variation of the active region. The AlSb/InAsSb/AlAsASb quantum well was used as the active region of the structure A. The layer thickness sequence in the QW is 10nm/20nm/50nm respectively.

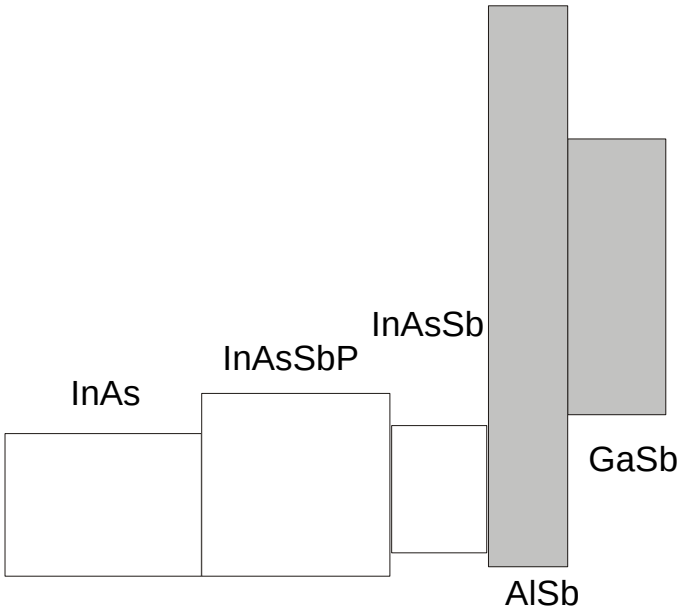

Fig.4.1. Schematic energy band diagram of the structure A grown by two-step MOCVD epitaxial method

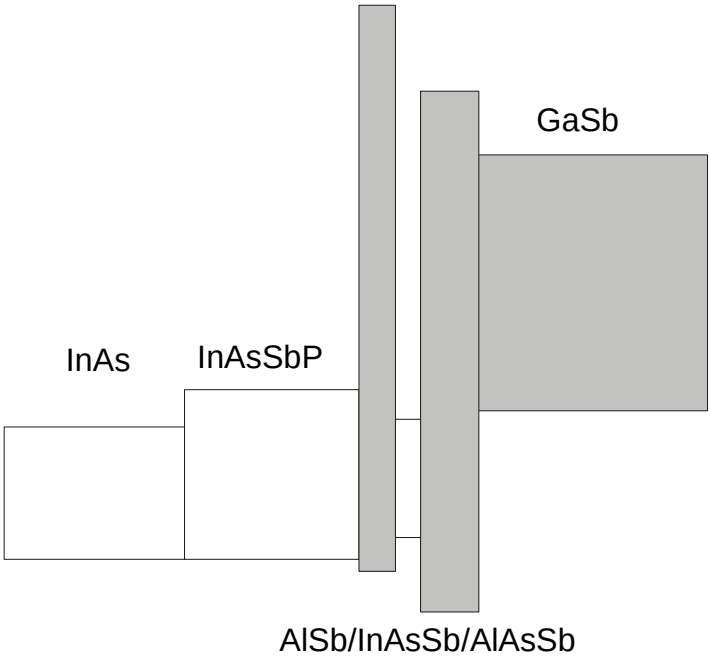

Fig.4.1. Schematic energy band diagram of the structure B (QW) grown by two-step MOCVD epitaxial method

4.2. Study of spontaneous emission

EL spectra for the heterostructures grown by combine method were obtained in the spectral range 0.25-0.55 eV at 77 K and 300 K. The low-temperature EL spectra of the structure A contained two pronounced emission bands with photon energy at maximum $h\nu_1^{77}$=0.370 eV and $h\nu_2^{77}$=0.485 eV (Fig.4.3). The average value of the bandwidth was

estimated to be $FWHM_1$=22 meV and $FWHM_2$=48 meV, respectively. In contrary to that the EL spectra at 300 K contained one pronounced emission bands with photon energy at maximum $h\nu_1^{300}$=0.342 eV whereas the second emission band at $h\nu_2^{300}$=0.435 eV was found as additional shoulder at the low-energy tail of the first peak. The FWHM of the first peak was about 65 meV.

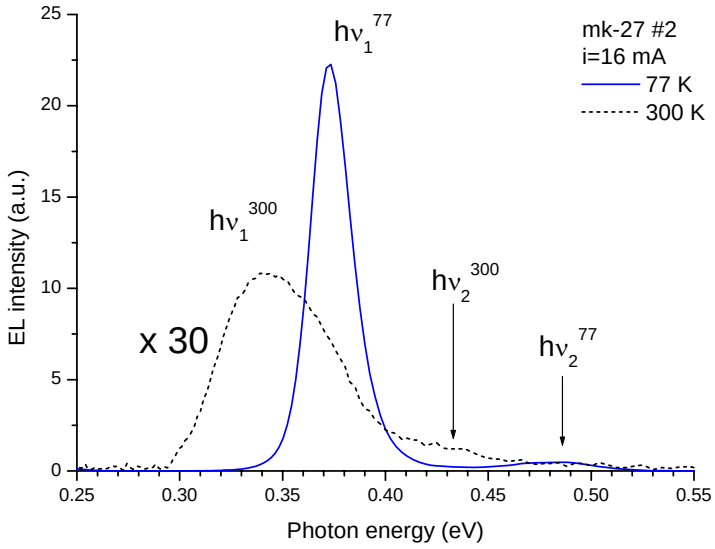

Fig.4.3. Comparison of EL spectra at 77 and 300 K for the asymmetric InAsSbP/InAsSb/AlAsSb heterostructure

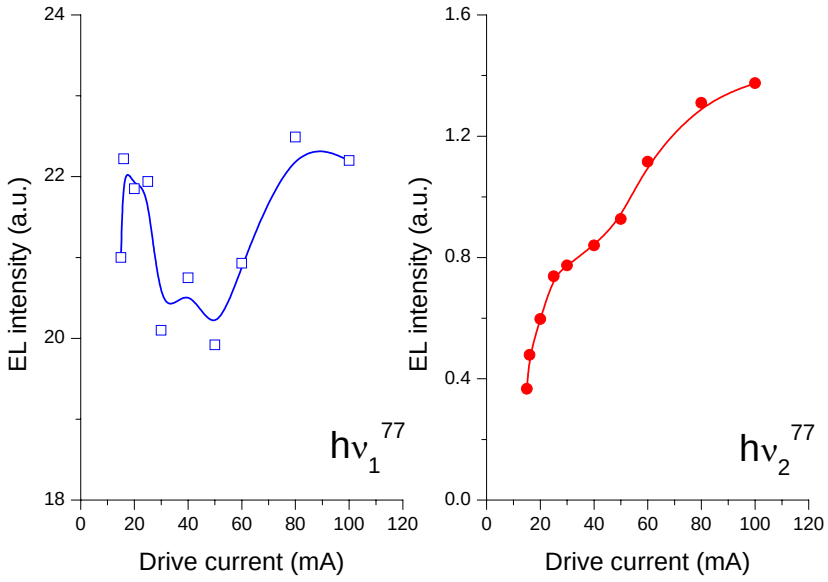

Fig. 4.4. Dependence of EL intensity on driving current for two emission bands at 77 K

The EL intensity at room temperature was 30 times lower than one at low temperature. The EL intensity depends on drive current nonmotonic. As it was shown in Fig.4.4 the local minimum in intensity for $h\nu_1^{77}$ emission band and the small drop for $h\nu_1^{77}$ were observed at the injection current i=50 mA. It should be noted that the spectral position

of $h\nu_1^{77}$ peak remains unchanged with the increasing of current injection while the blue shift toward higher energy by 6 meV was found for $h\nu_2^{77}$ peak (Fig.4.5). The spectral shift of the $h\nu_2$ band by 50 meV with temperature increasing from 77 K to 300 K is in a good correspondence with thermal variation of the energy gap of the InAs-based solid solution.

We suppose that the origin of the high-energy emission band is due to the radiative transitions of the hot carriers ejected from the narrow-gap active layer to the InAsSbP cladding layer with further recombination. In support to that assumption absorption bands of the water and carbon dioxide present in an atmospheric in the spectral range λ=2.6-2.7 μm were observed on the $h\nu_2$ peak.

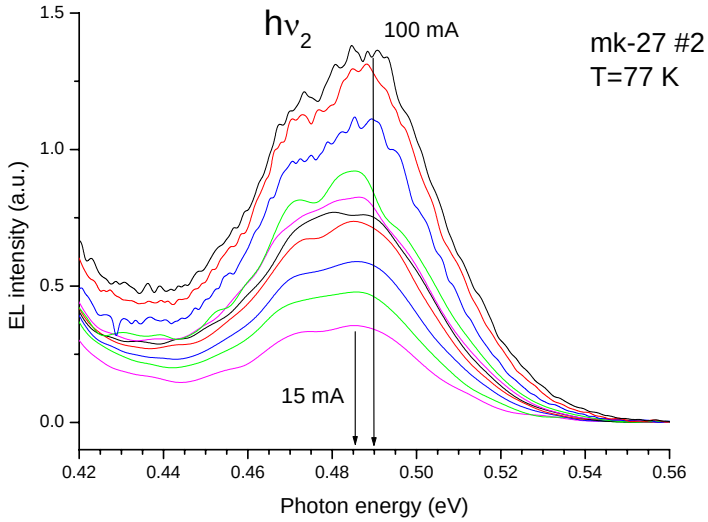

Fig.4.5. Evolution of $h\nu_2$ emission band on driving current at 77 K

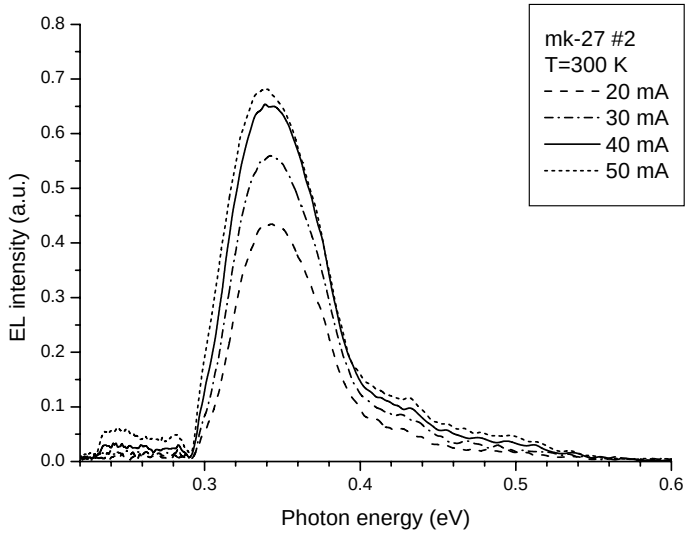

Fig.4.6. Evolution of EL spectra on driving current for the asymmetric InAsSbP/InAsSb/AlAsSb heterostructure at 300 K

The saturation of the EL intensity at room temperature and warming-up of the sample were found with drive current increasing (Fig.4.6). Again, at high injection level the luminescence in the wide-gap InAsSbP layer due to carrier leakage from the active region becomes visible.

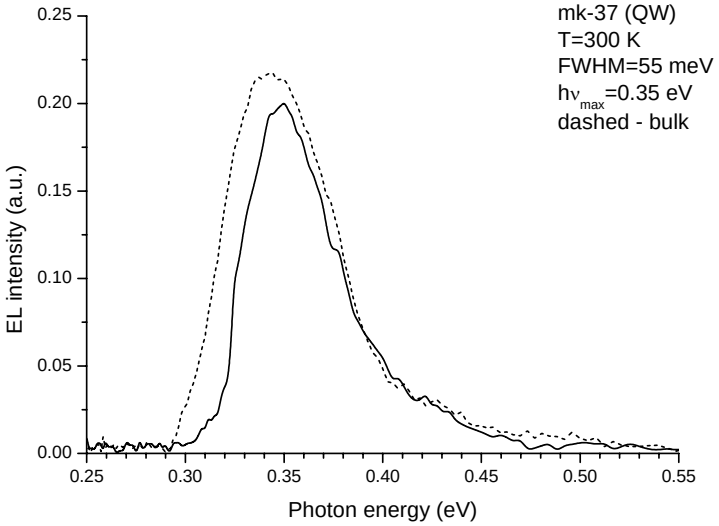

Fig.4.7. Comparison of EL spectra of the hybrid heterostructure based on bulk ternary InAsSb solid solution (dashed line) and AlSb/InAsSb/AlAsSb quantum well (solid line) in the active region at room temperature at fixed drive current Intensity for bulk layer is multiplied by factor of 0.5.

Fig.4.7 shows a small blue shift of the EL peak maximum towards higher energy for QW heterostructure in relative to interband radiative recombination in ternary InAsSb solid solution. It is obviously that the intensity of the interband radiative transitions was found stronger then one for single quantum well, however, the decreasing in bandwidth of the EL peak allows suggesting on a good holding of the carriers in quantum well at room temperature actually.

CONCLUSIONS

1. Asymmetric hybrid III-V/II-VI AlGaSb/InAsSb /CdMgSe laser structure was grown by combine two-technology methods: LPE (III-V part) and MBE (II-VI part).
2. Morphology of laser structures and surface potential profiles of the cleaved surface were studied by modified AFM method (Kelvin Probe Microscopy).
3. Spontaneous and coherent emissions of hybrid InAs/InAsSbP/InAsSb/CdMgSe laser structures were investigated. Intense electroluminescence was found in the range of 77-300 K. Lasing at λ=3.5 μm was achieved in pulse regime at 80 K. and threshold current density J_{th}=4 kA/cm^2 was obtained.
4. Optical confinement and spreading of the lasing in the active region of the hybrid InAsSbP/InAsSb/CdMgSe laser structure was computed.
5. Quantum well laser structures with single and triple AlSb/InAsSb/AlSb quantum wells were grown by MOVPE and their electroluminescence properties were studied in the range T=77-300 K. Characterization of these structures was made by Scanning Kelvin Probe Microscopy. Energy spectrum of the structures under study was theoretically estimated. Origin of radiative recombination transitions was analyzed. EL peaks can be ascribed to radiative transitions into the QW between the ground electron level and two occupied hole levels, respectively.
6. Theoretical computation of radiative and non-radiative recombination in an asymmetric quantum well was performed.
7. MOCVD technology was developed to growing InAsSb/InAsSbP double heterostructure with high phosphorus content (p<60%) in cladding layers. Photoluminescence and electroluminescence were studied at 77-300 K in dependence on P content in solid phase. Coherent emission at λ=3.1 μm for InAsSb/InAsSbP DH laser structure with high InP content in the cladding layers was observed at 77 K.
8. Wide-gap AlGaAsSb solid solution as confining layer for laser structure was grown on InAs substrate by MBE. Optimal temperature for planar growing was determined. Basic conditions of the epitaxial growth for InAs, InAsSb and AlGaAsSb solid solutions were established.
9. Original technology of the InAsSbP/InAsSb/AlAsSb heterostructure growing by combine two-steps MOCVD method was developed. The quantum well consisting AlSb/InAsSb/AlAsSb heterostructure with the thickness sequence of 10nm/20nm/50nm was used in an active region instead of the bulk InAsSb epilayer. Intense spontaneous emission was observed in the spectral range 0.25-0.55 eV at temperatures 77-300 K. This structure can be very attractive to design high-power mid-infrared lasers operating at high temperature.

FUTURE WORK RECOMMENDED

1. It is very interesting to prolong study of the new laser InAsSbP/InAsSb/Al(Ga)AsSb structure grown by two-steps MOVPE for design to high-power mid-ir lasers.
2. Coherent emission on single AlSb/InAsSb quantum well laser structure was not observed yet. However, the intense spontaneous emission in the range of 77-300 K was found. Taking into account the progress in fabrication of single and multiple QW heterostructures allows us to consider it as prospective active region of the mid-ir lasers.

3. Theoretical calculation of gain, optical power and maximum of operating temperature for QW mid-ir laser structure with various number of quantum wells will be performed.
4. Improvement of post-growth laser technology of the mid-ir laser and design optimization requires additional development.
5. Due to some technical problems with our MBE plant concerning to search of optimal source for antimonide epilayers in arsenide atmosphere, only a little attention was paid to quantum well AlGaSb/InAs structures grown by MBE.

In the beginning of this project submission we suppose to accomplish our complex study during two-year work and we have Work Plan on the second year too. Below we present corrected second year's Work Plan. We are able to start with this work from February-March 2005.

Work Plan on 2005-2006

V quarter. (March 2005 – May 2005)
Type II asymmetric GaAlAsSb/InAs(Ga,Sb)/InAsSbP laser structure growing by MOVPE
5.1. Growing of the asymmetric laser structure with the quantum well active region.
5.2. Characterization of the laser structures and interface quality (AFM, EPFM etc)
5.3. Theoretical calculation of wave function overlapping at the interface and carrier tunneling across heteroboundary

VI quarter. (June – August 2005)
Experimental and theoretical and experimental investigations of quantum well laser structures
6.1. Growing Al(As)Sb/InAsSb QW laser structures by MBE
6.2. Characterization of the laser heterostructures and interface quality
6.3. Experimantal and theoretical study of the radiative recombination transitions assisted by tunneling injection
6.4. Calculation of gain, optical power and maximum of operating temperature for laser structure with asymmetric confinement

VII quarter. (September – November 2005)
Improvement of post-growth technology for mid-IR hybrid laser structures
7.1. Design of mesa-stripe laser structures with various shapes of etched mesa profile
7.2. Fabrication of multi-layer Ohmic contacts with low resistivity ($<10^{-3}$ Ohm/cm)
7.3. Study of electroluminescence and current-voltage characteristics of the laser structures

VIII quarter. (December 2005– February 2006)
Comparative study of asymmetric hybrid quantum well laser structure growing by combine MOCVD and/or MBE methods
8.1. Investigation of spontaneous and coherent emissions, polarization properties of lasing spectra, temperature dependence of threshold current
8.2. Recommendation on laser design optimization
8.3. Final Technical Report and samples delivery

REFERENCES

1. P.Werle, Appl.Phys.Lett.1995, **60**, 499.
2. S.Civiš, A.P.Danilova, A.N.Imenkov, N.M.Kolchanova, V.V.Sherstnev , Yu.P.Yakovlev. Spectochemica Acta. PartA 2000, **56**, 2125
3. H.H.Gao, A.Kier, V.Sherstnev, Yu.P.Yakovlev. J.Phys. D: Appl.Phys.1999, **32**, 1768.
4. T.Miyashita, T.Manabe. IEEE, J.Quant. Electr. 1982, **QE-18**, 1432
5. Z.Fiet, D.Kostyk, R.J.Wood, P.Mac. Appl.Phys.Lett.1990, **57**, 2881.
6. G.G.Zegrya, A.D.Andreev. Appl.Phys.Lett.1995, **67**, 2681.
7. R.E.Kazarinov, M.P.Pinto. . IEEE, J.Quant. Electr. 1994, **QE-30**, 49
8. K.D.Moiseev, M.P.Mikhailova, O.G.Ershov, Yu.P.Yakovlev. Semiconductors, 1996, **30**, 223
9. Yu.Yakovlev K.Moiseev, M.Mikhailova, A.Monakhov, A.Astakhova, V.Sherstnev. SPIE 2000, Vol. **3947**, 144
10. Final Report for EOARD Contract F61775-99-WE-016. St.Petersburg, Ioffe Institute RAS, July 2000
11. Final Report for EOARD Contract 00-7036. (ISTC Project N 2044p) St.Petersburg, Ioffe Institute RAS, July 2003
12. S.V.Ivanov, K.D.Moiseev, V.A.Kaigorodov, V.A.Solovjev, S.V.Sorokin, B.A.Meltzer, E.A.Grebenshchkova, I.V.Sedova, Ya.V.Terentev, A.N.Semenov, A.P.Astakhova, M.P.Mikhailova, Yu.P.Yakovlev, P.S.Kop'ev, Zh.A.Alferov. Semiconductors, 2003, **37**, 223
13. S.V.Ivanov, V.A.Solovjev, K.D.Moiseev, A.A.Toropov, B.A.Meltzer M.P.Mikhailova, Yu.P.Yakovlev, P.S.Kop'ev. Appl.Phys.Lett.2001, **78**, 196.
14. H.Kpoemer 2004 Physica E-**20**, 194
15. S.S.Kizhaev, S.S.Molchanov, N.V.Zotova, B.V.Pushnyi, Yu.P.Yakovlev. J.Crist.Growth. 2003, **248**, 296
16. S.S.Kizhaev, S.S.Molchanov, N.V.Zotova, Yu.P.Yakovlev. IEEE Poc.Optoelectr. 2002, **149**, 36
17. T.V. L'vova, I.V. Sedova, K.L. Kostushkin, S.V. Sorokin, V.P. Ulin, V.L. Berkovits, and S.V. Ivanov, Abstracts XXVI Workshop on Compound Semiconductor Devices, Chernogolovka, p.67 (2002).
18. V. L. Berkovits, V. P. Ulin, D. Paget, J. E. Bonet, T. V. L'vova, P. Chiaradia, and B. M. Lantratov, J. Vac. Sci. Technol. A **16**, 2528 (1998).
19. S.V. Ivanov, A.A. Toropov, I.V. Sedova, V.A. Solovyev, Ya.V. Terentyev, V.A. Kaygorodov, M.G. Tkachman, P.S. Kop'ev, and L.W. Molenkamp, J. Cryst. Growth, 2001, **227**, 693)
20. A.Ankudinov, V.Evtikhiev, E.Kotelnikov, A.Titkov and R. Laiho J. Appl. Phys. 2003, **93**, 432
21. A.V. Ankudinov, V.P. Evtikhiev, B.G. Koshajev, D.K. Nelson, A.S. Shkolnik A.N. Titkov Proc. Intern. Workshop SP-2004, Nizhny Novgorod, Russia May 2-6 2004, p.23
22. A.S. Polkovnikov, G.G. Zegrya Phys. Rev. B, 1998, **58,** 4039
23. S. S. Kizhaev, Ph.D Thesis, Ioffe Institute St. Petersburg, Russia, 2004
24. D. Wu, B. Lane, H. Mohseni, J. Diaz, and M. Razeghy Appl. Phys. Lett., 1999, **74**, 1194

Publications In the frame of project

1. S.S.Kizhaev, S.S.Molchanov, N.V.Zotova, B.V.Pushnyi, Yu.P.Yakovlev. Powerful InAsSbP/InAsSb light emitting diodes grows by MOVPE. J.Crist.Growth. 2003, **248**, 296

2. A.P.Astakhova, N.D.Ilinskaya, A.N.Imenkov, S.S.Kizhaev, S.S.Molchanov, Yu.P.Yakovlev. Interfase and interband laser generation in InAs/InAsSbP heterostructure grows by MOVPE. Semiconductors 2004 to be published
3. K.D.Moiseev, A.P.Astakhova, G.G.Zegrya, M.P.Mikhailova, Yu.P.Yakovlev, E.Hulicius, A.Hospodkova, J.Pangrac, T,Simeĉek. Electroluminescence properties of quantum well AlSb/InAsSb heterostructures grown by MOVPE. Proc. 12th Int.Symp. Nanostructures: Physics and Technology, St.Petersburg, Russia June 2004 p.58
4. K.D.Moiseev, A.P.Astakhova, E.V.Ivanov, G.G.Zegrya, M.P.Mikhailova, Yu.P.Yakovlev, E.Hulicius, A.Hospodkova, J.Pangrac, T,Simeĉek. Quantum well AlSb/InAsSb laser heterostructures grown by MOVPE. Book of Abstracts 6th Int.Conf. MIOMD-VI, St.Petersburg, Russia June 28-July 2 2004 p.45
5. A.Titkov, P.Girard, A.Ankundinov, M.Ramonda. Scanning Kelvin probe Microscopy of the mid infrared lasers. . Book of Abstracts 6th Int.Conf. MIOMD-VI, St.Petersburg, Russia June 28-July 2 2004 p.54
6. A.Titkov, P.Girard, A.Ankundinov, M.Ramonda, B.Kosheav. Quantative Scanning Kelvin probe Microscopy Semiconductor device heterostructures. Abstracts of 6th Seminar Nanoscale 2004, Braunschweig, Germany, March 25th-26th, 2004
7. A.P.Astakhova, N.D.Ilinskaya, A.N.Imenkov, S.S.Kizhaev, S.S.Molchanov, Yu.P.Yakovlev. Simultaneously interfase and interband laser generation in InAs/InAsSbP heterostructure grown by MOCVD. Tech.Phys.Lett 2004, **12**, 1024
8. K.D.Moiseev, E.V.Ivanov, A.N.Imenkov, M.P.Mikhailova, Yu.P.Yakovlev. Mid-infrared (λ=3.5μm) hybride InAsSbP/InAsSb/CdMgSe laser grown by combine LPE+MBE technology, Semiconductors, to be published.
9. K.D.Moiseev, A.P.Astakhova, E.V.Ivanov, G.G.Zegrya, M.P.Mikhailova, Yu.P.Yukovlev, E.Hulicius, A.Hospodkova, J.Pangrac, T,Simeĉek. Electroluminescence properties of AlSb/InAsSb/AlSb quantum well heterostructures grown by MOVPE. J.Appl.Phys. to be published